Isotopic evolution of Mauna Loa and the chemical structure of the Hawaiian plume

Donald J. DePaolo

Center for Isotope Geochemistry, Department of Earth and Planetary Science, University of California, Berkeley, California, 94720-4767, USA (depaolo@socrates.berkeley.edu)

Also at Earth Sciences Division, E.O. Lawrence Berkeley National Laboratory, Berkeley, California 94720, USA

Julia G. Bryce

Center for Isotope Geochemistry, Department of Earth and Planetary Science, University of California, Berkeley, California, 94720-4767, USA (jbryce@uclink4.berkeley.edu)

Allen Dodson

Center for Isotope Geochemistry, Department of Earth and Planetary Science, University of California, Berkeley, California, 94720-4767, USA

Now at The College of Wooster, Wooster, Ohio 44691, USA (adodson@acs.wooster.edu)

David L. Shuster

Center for Isotope Geochemistry, Department of Earth and Planetary Science, University of California, Berkeley, California, 94720-4767, USA

Also at Earth Sciences Division, E.O. Lawrence Berkeley National Laboratory, Berkeley, California 94720, USA

Now at Division of Geological Planetary Sciences, California Institute of Technology, Pasadena, California 91125, USA (dshuster@gps.caltech.edu)

B. Mack Kennedy

Center for Isotope Geochemistry, Department of Earth and Planetary Science, University of California, Berkeley, California, 94720-4767, USA (mkennedy@ux5.lbl.gov)

Also at Earth Sciences Division, E.O. Lawrence Berkeley National Laboratory, Berkeley, California 94720, USA

[1] **Abstract:** New He isotopic data from the HSDP pilot hole core, lava accumulation rate models, and data from the literature are used to develop a 200,000 year isotopic record for the lava erupted from the Mauna Loa volcano. This record, coupled with an analogous record from Mauna Kea from the Hawaii Scientific Drilling Project (HSDP) pilot hole project and other literature data from the GEOROC database, are used to construct a "map" of lava isotopic compositions for the island of Hawaii. The isotopic map is converted to a map of the He and Nd isotopic compositions of melts from the mantle plume, which can be compared with a published melt supply map derived from geodynamic modeling. The resulting map of the plume indicates that values of helium $^3He/^4He > 20$ Ra are confined to the core of the plume (radius ≈ 20–25 km) and correspond to potential temperatures $>1565°C$, suggesting the He isotopic signal is derived from deep in the mantle. The $^3He/^4He$ map has closed contours down to 10 Ra; the contours are teardrop-shaped and elongated in the general direction of plate motion. The closed contours indicate that most of the plume He signal is lost during the early

stages of melting, which is consistent with helium behaving as a strongly incompatible element ($K_{He} \leq$ 0.001). The ε_{Nd} contours (and by inference the contours for Sr, Pb, Hf, and Os) do not all close on the scale of the island of Hawaii but instead partially follow material flow lines within the plume beneath the lithosphere. The plume signal for Nd extends circa 100 km in the direction of plate motion, which is consistent with the moderately incompatible behavior of Nd ($K_{Nd} \approx 0.02$). Downstream from the plume core epicenter, plume Nd occurs with asthenospheric He; this could be mistaken for an additional plume component, whereas it may be only a manifestation of differing incompatibility. Data from Mauna Loa suggest the presence of a low-^{3}He/^{4}He plume component that has low ε_{Nd} and high ^{87}Sr/^{86}Sr. The plume map suggests that this component may be a blob (circa 20 km scale), located between Mauna Loa and Hualalai and separated from the main plume core by a zone of more asthenosphere-like material. The HSDP data preclude a proposed model where this material represents a ring of entrained material from the lower mantle. The orientation of the elongation of contours on the plume He and Nd isotope maps ($\sim$N45°W) does not match the modern plate motion as measured by GPS (N65°W) nor does it match the trend of the ridge axis between Maui and Loihi (N30°W). The geochemical evidence, as well as the locations and growth histories of the Hawaiian volcanoes, suggest that the plume, as well as the Pacific plate, has been moving at a velocity of several centimeters per year over the past 1 to 2 million years.

1. Introduction

[2] There is general consensus that mantle plumes are responsible for the production of midplate linear island chains and other forms of oceanic island volcanism. The standard conceptualization of mantle plumes is of cylindrical jets of abnormally hot mantle rock material ascending approximately vertically beneath the lithosphere [e.g., *Watson and McKenzie*, 1991]. Fluid dynamical models of plumes show they should be axisymmetric with respect to temperature, with a particularly high temperature core [*Kellogg and King*, 1997; *Hauri et al.*, 1994; *van Keken*, 1997]. It is also typically the case that the geochemical and petrological structure of a plume is assumed to be axisymmetric [e.g.,

Hauri et al., 1996; *Lassiter et al.*, 1996]. The interaction of a plume with moving lithosphere should cause a plume to become deformed in the uppermost mantle [e.g., *Ribe and Christensen*, 1994, 1999], such that some aspects of symmetry would be modified. The passage of a plume through a convecting lower mantle may also cause the plume's upward path to deviate substantially from vertical [*Steinberger and O'Connell*, 1998].

[3] Although the radially symmetric plume (in the geochemical sense) is a simple and useful construct, there is little direct evidence that such structure exists [*Geist et al.*, 1999; *Kurz and Geist*, 1999; *Hoernle et al.*, 2000]. The Hawaiian plume, by virtue of its size and the

amount of supporting information, should be the best place to test models for plume structure. Hawaiian volcanoes provide evidence that the Hawaiian plume is zoned in terms of temperature and melting rate. The eruption rate of the volcanoes is a function of the distance of their summits from the presumed location of the plume core [*Lipman*, 1995; *DePaolo and Stolper*, 1996]. Existing U-Th-Ra isotopic data also support the model of a concentrically zoned plume in terms of upwelling and melting rates [*Sims et al.*, 1999]. Models put forth for the Hawaiian plume geochemical structure consist of a quasi-concentrically zoned plume with "enriched" material from the plume source region at the core, surrounded by entrained "depleted" mantle. The source of the entrained material remains a topic of debate, with some workers identifying it as asthenospheric mantle [*Kurz et al.*, 1996] and others identifying it as lower mantle plus asthenospheric mantle [*Hauri et al.*, 1996; *Lassiter et al.*, 1996]. Some observations made at Hawaii, however, seem to be inconsistent with the axisymmetric plume structure. An example is the identification of the so-called "Loa" and "Kea" geochemical trends [*Frey and Rhodes*, 1993]. The Kea trend volcanoes (including Mauna Kea) are lined up such that they appear to have traversed the northeastern part of the plume top, whereas the Loa trend volcanoes (including Mauna Loa) have traversed the southwest half of the plume and passed closer to the plume axis. The distinction between these two volcanic chains does not preclude radial structure but nevertheless seems to suggest northeast-southwest asymmetry.

[4] The geochemical structure of mantle plumes can potentially be evaluated using geochemical data from volcanoes associated with mantle plumes. It might be expected that as the hot spot volcanoes drift over a mantle plume, the erupted lava will change character with time (and hence with position relative to the axis of the plume). If there is axisymmetric geochemical structure, this should be evident in time-dependent geochemical changes in the lava erupted from each volcano. The Hawaii Scientific Drilling Project [*Stolper et al.*, 1996] was undertaken in part to assemble a sufficient database to provide such a test of the Hawaiian plume structure. The pilot phase of this project returned core material from both Mauna Loa and Mauna Kea volcanoes from the vicinity of Hilo. The stratigraphic progression available from the core represents a systematic sampling of the lava output with time and hence is useful for evaluating plume structure. The primary efforts of the data collection phase of the pilot project focused on the Mauna Kea part of the section.

[5] In this paper, we review the data collected on the Mauna Loa part of the section, present new He, Nd, Sr, and Pb isotopic data, and evaluate those data in conjunction with the Mauna Kea data and other data from Hawaii in terms of plume structure. In relating the isotopic data to plume structure we use aspects of the dynamical model of *Ribe and Christensen* [1999]. The Ribe and Christensen numerical model provides a three-dimensional picture of the Hawaiian plume, in which the distribution of temperature, flow velocity, melting rate, and magma production are represented. The model is valuable because it contains enough of the plume and lithosphere physics to allow us to move beyond cartoons to represent the plume. In particular, it allows us to relate the spatial distribution of isotopic anomalies to the spatial distribution of temperature anomalies. It also indicates the effects of lithosphere flow on the plume structure, provides information on the structure of magma production functions as they apply to volcano growth, and provides estimates of the total aggregate extent of melting and its distribution within the plume. As discussed below, the size of the melting region for the *Ribe and Christensen* [1999] model is

probably too large owing to their particular selection of input parameters. This aspect of their model is not used, but it does not invalidate the other features of the model at the level we need them for our analysis.

2. Volcano Tracks and Ages of the Samples

[6] Each volcano in the Hawaiian chain drifts northwestward (relative to the Hawaiian plume) as it is carried by the Pacific plate. The modern velocity of this drift is thought to be in the neighborhood of 9 cm/yr [*Clague*, 1996], although recent GPS measurements suggest a value of 7 cm/yr for the absolute velocity of the Pacific plate, and some estimates in the literature are as high as 13 cm/yr [*Moore and Clague*, 1992]. As one samples down-section through older lava flows in a drill core (or canyon wall, fault scarp, etc.) derived from a single volcano, the characteristics of the lava as a function of age correspond to a "track" across the mantle plume.

[7] The inferred tracks followed by each of the volcanoes of the Island of Hawaii are shown in Figure 1. The tracks shown are along a trend of N30°W and tick marks are for a velocity of 9 cm/yr. The choices of values for the trend and velocity are discussed further below. Overlying the tracks are the melt supply model of *Ribe and Christensen* [1999] in Figure 1a and the melt supply model of *DePaolo and Stolper* [1996] in Figure 1b. These maps are used as a framework for the interpretation of the isotopic data presented later in this paper. The location of the plume axis, or the zone of maximum melt production, was chosen so that in the direction perpendicular to the plate motion vector (the northeast-southwest direction), the plume axis lies along the axis of the Hawaiian Ridge as defined by seismic refraction data [*Moore*, 1987] (see Figure 10 below). In the direction parallel to plate motion the

melting zone is arranged so that Mauna Loa has passed over ~80% of the main melting region, Loihi has passed over ~20% of the melting region, and Kilauea has the highest magma supply of the active volcanoes. As discussed by *DePaolo and Stolper* [1996], this arrangement is consistent with the recent lava accumulation rate of Mauna Loa and the present volume of Loihi.

[8] In order to reconstruct the position of the volcanoes corresponding to a particular lava sample, the age of the lava sample must be known. Samples from Mauna Loa volcano that have been analyzed for He and other isotope ratios vary in age from historical (<200 years) to ~200,000 years (200 ka). Direct geochronological determinations of the lava flow ages, however, are mostly limited to samples that are within the range of radiocarbon dating, which is 40 ka or less [*Kurz and Kammer*, 1991; *Beeson et al.*, 1996; *Lipman and Moore*, 1996]. In this paper we attempt to place all of the available samples from Mauna Loa in a consistent chronological framework using the lava accumulation rate model of *DePaolo and Stolper* [1996] and the known "depth" of all of the samples relative to the present surface of Mauna Loa. In the following paragraphs we discuss some issues relating to the construction of lava accumulation rate models, the depths of the undated samples relative to the modern surface of Mauna Loa, and the available geochronologic data.

[9] Calculation of lava accumulation rates for a particular volcano requires a model for the magma supply to the volcano, coupled with a model for the surface area of the volcano as a function of time. The model used here [*DePaolo and Stolper*, 1996] (see Figure 1b) is based on the radially symmetric plume model of *Watson and McKenzie* [1991]. The curve of magma supply versus time for an individual volcano is assumed to have a quasi-Gaussian
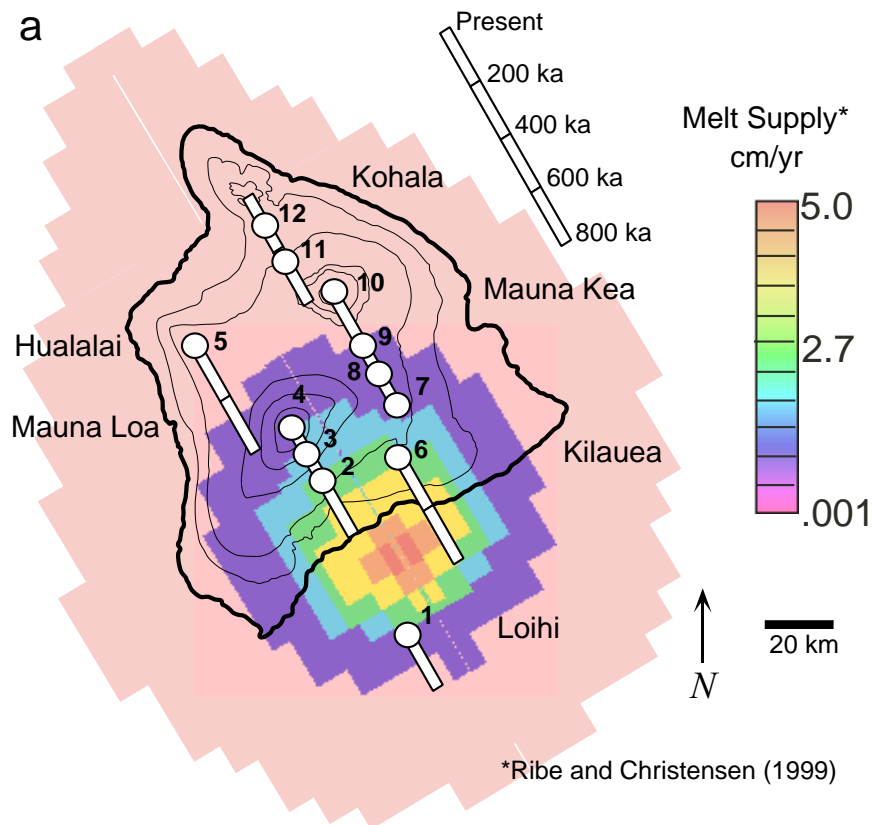
a

Figure 1. Map of Hawaii showing volcano locations superimposed on the (a) map of melt supply calculated by *Ribe and Christensen* [1999]. The melt supply units have been converted to centimeter per year from the units originally used. (b) After Figure 1a using the melt supply model of *DePaolo and Stolper* [1996]. In both Figures 1a and 1b also shown are the positions of each of the volcano summits as function of time in the geologic past, assuming a Pacific plate velocity of 9 cm/yr. The melt supply map of Figure 1a is placed so that its axis of symmetry has an orientation of N30°W and is centered on the axis of the Hawaiian Ridge as defined by seismic refraction data [*Moore*, 1987]. The main melt supply region (bounded approximately by the 2 cm/yr contour) is centered between Mauna Loa and Loihi, which provides the best fit to the modern lava accumulation rates for Mauna Loa and the historical eruption rate of Kilauea. The numbered locations correspond to volcano positions for which isotopic data are listed in Table 2. These data come partly from Figures 4 and 5 and form the basis of the geochemical maps shown in Figures 7 and 8.

shape and is adjusted in amplitude to account for the path of the volcano over the plume and in duration to account for the plate velocity. The dimensions of the melting region are constrained by the present positions and eruption rates of the volcanoes. In map view, the *Ribe and Christensen* [1999] magma supply model (Figure 1a) differs from the *DePaolo and Stolper* [1996] model (Figure 1b) in that the

magma supply contours have radial asymmetry and larger radii. The asymmetry is not large but presumably is a more accurate representation of the shape of the melt production region than is the *DePaolo and Stolper* [1996] model. When the Ribe and Christensen map is used to generate curves of magma supply versus time for a single volcano, the shapes of the curves are nearly identical to those used by *DePaolo and*
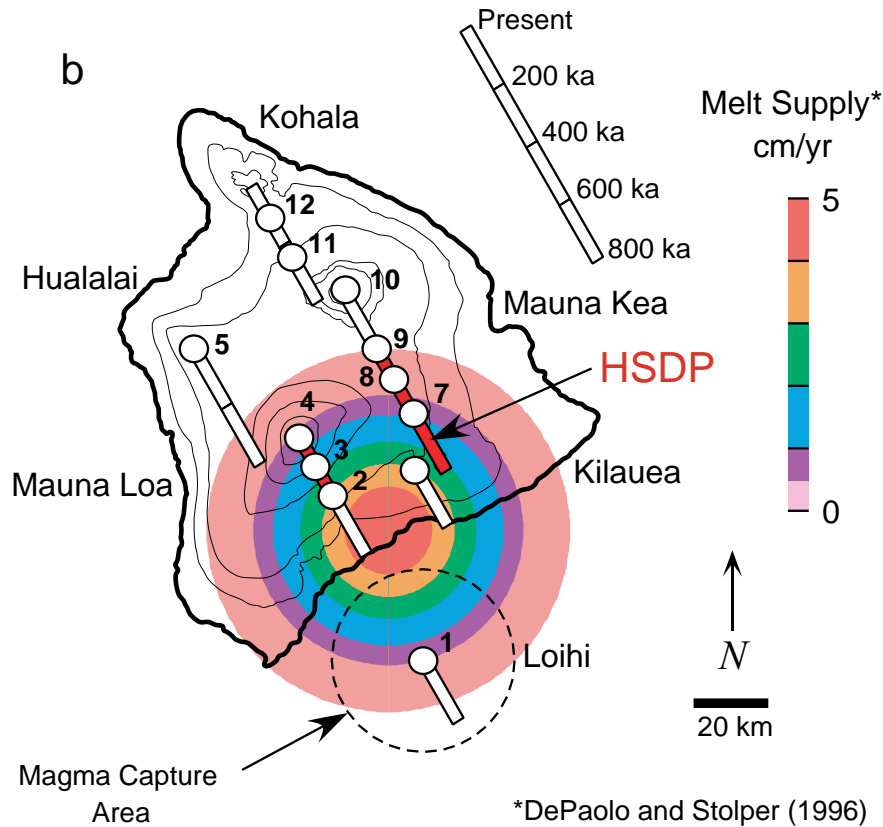
Figure 1. (continued)

Stolper [1996], but they are 50% wider. The increased width is not consistent with the data available on the lifetimes and current eruption rates of the Hawaiian volcanoes, so we have chosen not to use the Ribe and Christensen model magma supply values to calculate lava accumulation rates. The size of the melting region calculated for the Ribe and Christensen model depends on the formulation used for the mantle solidus and the temperature dependence of mantle viscosity. A lower solidus temperature at 3–5 GPa (compare *Walter* [1998] and compilations by *Hirschmann* [2000] and *Herzberg et al.* [2000]) or an increased temperature dependence of viscosity (N. M. Ribe, personal communication, 2001) would narrow the melting region. For the present purposes, the *DePaolo and Stolper* [1996] model appears

adequate for estimating lava accumulation rates. The shape of the magma production function is compatible with the Ribe and Christensen model. The model can also account well for the volumes and ages of the seven volcanoes (including Mahukona [*Moore and Clague*, 1992]) that make up the island of Hawaii. The model is consistent with the measured lava accumulation rates of Mauna Kea over the past 400 kyr [*Sharp et al.*, 1996], the inferred accumulation rates for Mauna Loa and Kilauea over the past 100 kyr [*Lipman*, 1995], the inferred present eruption rates of Mauna Loa and Kilauea [*Lipman*, 1995], and the present size of Loihi.

[10] The ages and/or stratigraphic positions of all of the analyzed Mauna Loa samples are quite well constrained. The data of *Kurz et al.*
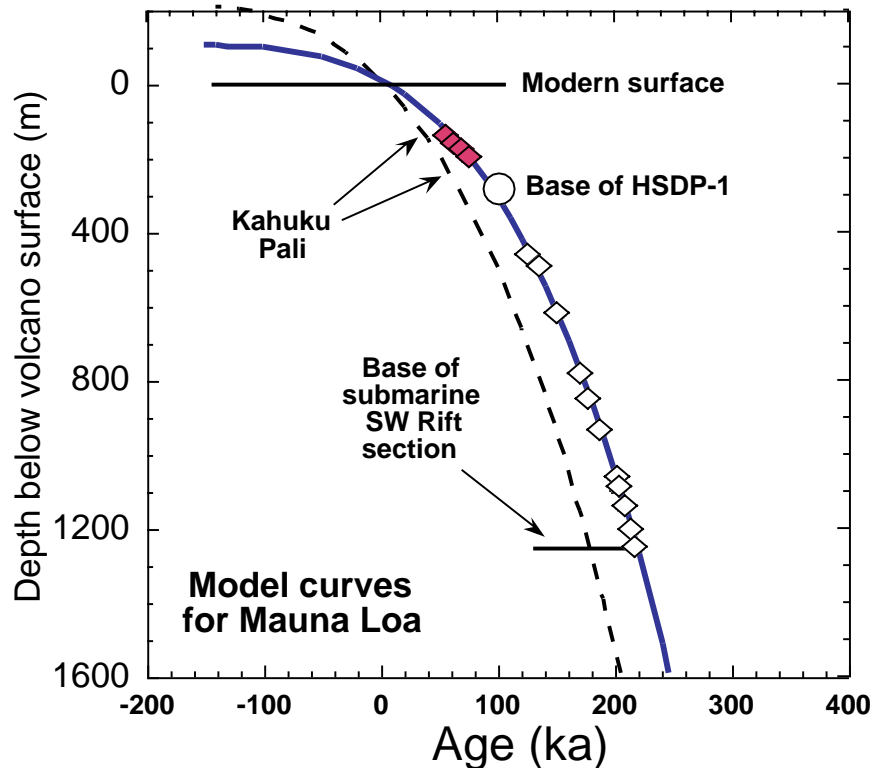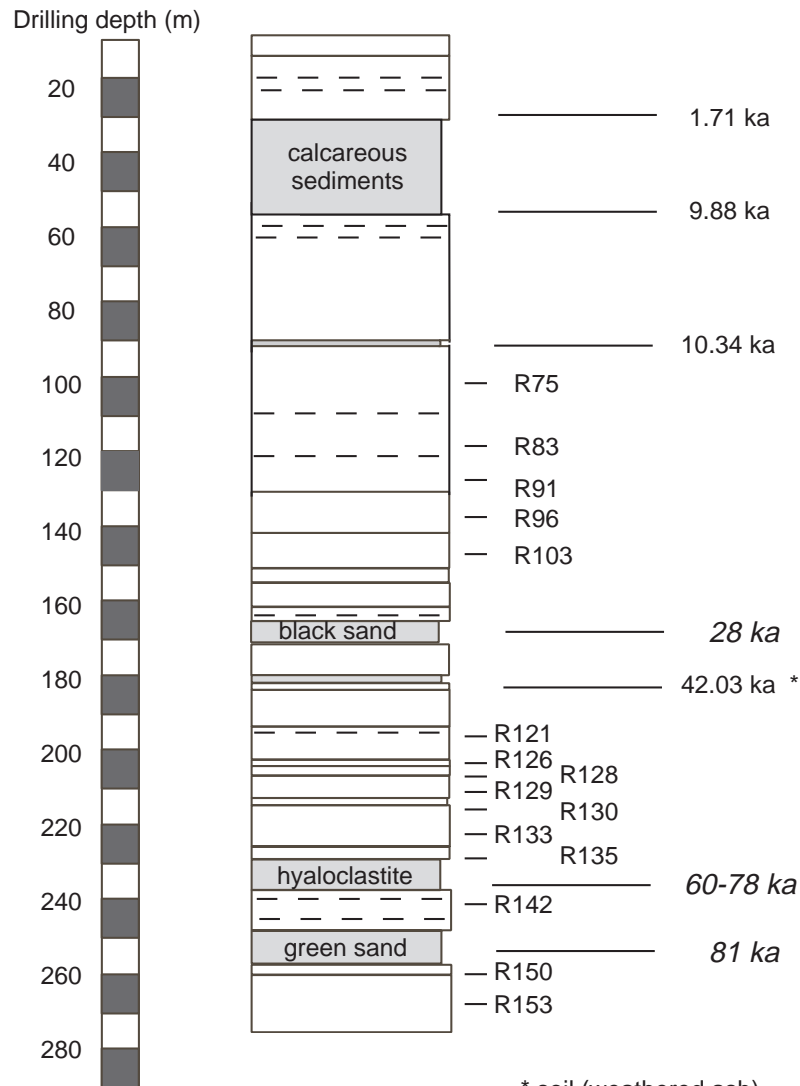
Figure 2. Model age versus depth for Mauna Loa volcano. The volcano growth curves were constructed for Mauna Loa [after *DePaolo and Stolper*, 1996]. The curve on the right (marked with diamonds) is calculated with the endpoint for Mauna Loa occurring in 200 kyr. This curve was used to determine model ages for the samples discussed below and depicted in Figures 3 and 4. The curve on the left, for comparison, is calculated using an endpoint for Mauna Loa set 150 kyr in the future. Plotted on the left curve are the relative stratigraphic positions of the subaerial Kahuku samples (solid diamonds) and the submarine Mauna Loa rift samples (open symbols) of *Kurz et al.* [1995].

[1995] represent lava samples taken from the headwall scarp of a large submarine landslide. These samples were placed in stratigraphic order by the authors on the basis of geographic coordinates and the depth below sea surface at which they were collected. Each sample was assigned a stratigraphic "depth" relative to the present volcano surface. The *Kurz et al.* [1995] samples are not dated. The ages are assigned using the lava accumulation rate model of *DePaolo and Stolper* [1996] as shown in Figure 2. The samples from the HSDP pilot hole can be placed in stratigraphic order based on depth in the hole and assigned ages based on the radiocarbon, U-Th, and ^{40}Ar-^{39}Ar ages that

were determined for interlayered carbonate and peat and a lava sample from near the bottom of the section (Figure 3). The available data indicate that the age of the lava section at a depth of 280 m is ~100 ka [*Sharp et al.*, 1996]. There are also numerous ^{14}C-dated horizons between 0 and 40 ka [*Beeson et al.*, 1996; *Lipman and Moore*, 1996] and a beach deposit that can be dated using the subsidence rate and a Late Pleistocene sea level curve. For the HSDP samples we believe that the assigned ages are accurate to within about ±5% of the age for the samples of age 50 ka or less and about ±10% for the older samples. Accumulation rates for Mauna Loa have also been estimated from

HSDP Pilot Drill Core
Sample Stratigraphy of Mauna Loa lavas

Figure 3. Schematic stratigraphic reconstruction of the Mauna Loa portion of the HSDP Pilot Hole. Tholeiitic basalt units are represented by white boxes; heavily dashed lines represent internal flow boundaries within the units. Sedimentary units are stippled gray. Ages marked are ^{14}C dates provided by *Moore et al.* [1996] and *Beeson et al.* [1996]; italicized dates are based on subsidence reconstruction models of *Lipman and Moore* [1996].

Table 1. Isotopic Data for Mauna Loa Lavas (HSDP Pilot Core)

Sample	Depth, m	^{3}He/^{4}He (R/Ra)[a]	±	^{87}Sr/^{86}Sr[b]	ε_{Nd}[c]	^{206}Pb/^{204}Pb	^{207}Pb/^{204}Pb	^{208}Pb/^{204}Pb[d]
R75-1.7	105	9.18	0.93	0.703892	5.78	18.109	15.466	37.870
R83-3.9	118	9.62	0.74	0.703904	6.17	18.094	15.465	37.820
R91-2.3	129	11.52	0.29	0.703741	6.73	18.276	15.487	38.044
R96-1.8	137	10.94	0.94	0.703765	6.84	18.258	15.470	37.995
R103	148	10.39	0.88					
R121-2.45	192	13.93*	0.36	0.703761	6.82	18.259	15.482	37.971
R126-0.9	200	11.57*	0.84	0.703730	6.63	18.225	15.471	37.980
R128-0.45	206	11.50	0.29	0.703880	6.04	18.035	15.495	37.784
R128-6.4	208	11.43*	0.21					
R129-5.5	211	11.42	0.23					
R130-4.65	214	11.25*	0.10					
R130-8.4	215	14.80*	0.29					
R133-6.1	223	14.22	0.51					
R135-3.5	230	15.32	0.39					
R142-1.6	243	14.72	0.79					

[a] R/Ra is the ratio of measured ^{3}He/^{4}He in the sample to atmospheric value of 1.4×10^{-6}. Measurements without asterisks are not blank corrected. The He data for these samples were measured in analog mode with the ^{4}He peak analyzed on the Faraday cup and the ^{3}He peak analyzed on an electron multiplier. Line blanks measured during the course of the analyses of these samples had levels of ^{4}He undetectable above the machine's background (see text and *Dodson et al.*, 1998 for discussion); maximum blank correction on the measurements denoted by asterisks was <0.4 R/Ra. During the course of these analyses an air standard with a measured ^{3}He/^{4}He value of $1.40 (\pm 0.08) \times 10^{-6}$ and a He standard with 2.40 ± 0.15 R/Ra were run repeatedly to monitor machine performance.

[b] Analytical uncertainty on ^{87}Sr/^{86}Sr measurement is ≤ 0.000015. See text for discussion.

[c] Here ε_{Nd} calculated from $10^4 \times [(^{143}Nd/^{144}Nd)_{meas}/(^{143}Nd/^{144}Nd)_{CHUR} - 1]$. CHUR = 0.511836, based on $^{146}Nd/^{142}Nd = 0.636151$. Analytical uncertainty on Nd measurements is ≤ 0.000010 or $\sim 0.2 \varepsilon$ units.

[d] Pb measurements corrected for mass fractionation by average value of 0. 08%/amu. An average of 12 NBS-981 measurements, taken throughout the course of the HSDP pilot samples analyses, with 2 SE(M): ^{208}Pb/^{204}Pb; 36.565 (0.039), 15.446 (0.013), and 16.903 (0.010).

geological data [e.g., *Lipman*, 1995; *Lipman and Moore*, 1996; *Moore et al.*, 1996]. The lava accumulation rate for Mauna Loa on its lower slopes is estimated to be 2–3 mm/yr averaged over the last 100 kyr [*Lipman and Moore*, 1996].

3. Sample Descriptions and Analytical Techniques

[11] The Mauna Loa basalts analyzed in this study (Figure 3, Table 1) are a subset of those cored in the pilot hole phase of the Hawaii Scientific Drilling Project (HSDP). The selected samples are taken from the core recovered from drilling depths of ∼105 to ∼210 m. Samples are tholeiitic basalts [*Rhodes*, 1996], containing between 10 and 32% olivine phe-

nocrysts by volume [*Baker et al.*, 1996]. For the noble gas analyses, olivine phenocrysts (>1 mm typically) were handpicked from coarsely crushed core samples. Helium was released from the samples by in vacuo crushing, which minimizes in situ cosmogenic and radiogenic contributions (see *Kurz* [1986] for discussion). Samples of olivine of approximately one gram were loaded into a manual mortar-and-pestle attached to a noble gas processing line [see *Dodson et al.*, 1998]. The line was baked and pumped for 24 hours at 200°C. Following this pumping period, with the sample in the crushing apparatus, blanks were processed and analyzed in the same manner as the sample but without crushing the sample. The samples were crushed for ∼5 min to release the noble gases. Reactive gases were removed using a series of

Zr-V-Fe and Zr-Al getters, leaving the remaining noble gases to be adsorbed onto activated coconut charcoal cooled to $\sim$30 K. The charcoal was then warmed to 40 K to release He gas, separately from the other noble gases, which was then introduced into the mass spectrometer for analysis. Isotope measurements were made on a VG5400 mass spectrometer equipped with a Faraday cup (for ^{4}He) and an electron multiplier (for ^{3}He). Two different methods were used for the helium isotope analyses. For most of the samples the ^{4}He was measured on the Faraday cup and the ^{3}He on the electron multiplier in analog mode (gain $\sim$10^7). In these cases the ^{4}He blanks were below detection limits, as measured on the Faraday cup and the background at mass ^{3}He was <5% of the ^{3}He peak heights measured for the samples. For these samples the helium isotopic data have not been corrected for blank contributions. For the remaining five samples (marked with an asterisk in Table 1), both the ^{4}He and ^{3}He were measured on the electron multiplier that was operated in ion counting mode. The helium isotopic data for these samples have been corrected for measured blank contributions. The maximum correction was <0.4 Ra. The dead-time correction for ^{4}He was <2%. Machine performance and mass fractionation were evaluated by measuring aliquots of air and a reference sample of He gas prepared by Spectra Gases Inc.

[12] For the Sr-Nd-Pb analyses the samples were split into pea-sized chips and then leached in 3 M HCl. The chips were then powdered. For the Sr and Nd work, the powders were further leached in 3 M HCl. Aliquots ($\sim$50 mg) of the prepared powders were then digested in HF-HClO$_4$ mixtures. Standard ion chromatographic procedures were then employed for element separation [e.g., *DePaolo*, 1978]. Purified Sr salts were loaded in Ta$_2$O$_5$ on rhenium filaments for analysis. Nd salts were loaded in HNO$_3$ onto rhenium filaments, and then Nd

was run as NdO$^+$ in an environment $\sim$10^{-6} mbar oxygen pressure. Isotopic analyses were performed at the Berkeley Center for Isotope Geochemistry using a VG Instruments Sector 54-E multicollector mass spectrometer. Nd and Sr measurements were made in dynamic mode. Nd isotopic compositions were normalized to ^{146}Nd/^{142}Nd = 0.636151 and are reported in this study relative to the chondritic uniform reservoir (CHUR) value of 0.511836. Standards were run over the course of the analyses, with mean measurements of 0.511842 (5) for BCR-1 and 0.710283(18) for NBS-987.

[13] For the Pb analyses, $\sim$200 mg aliquots of powdered samples were dissolved in a HF-HClO$_4$ mixture and then brought into solution in a HCl-HBr mix. Standard laboratory procedures [e.g., *Getty and DePaolo*, 1995] were employed for lead extraction. Procedural lead blanks during the course of this study were less than $\sim$1 ng, insignificant for the amount of lead processed in these samples. Isotopic measurements were made in static mode on the multicollector mass spectrometer. Twelve measurements of NBS-981 were made over the time period these samples were analyzed (see Table 1). The average of these NBS-981 values was then used to calculate in-run fractionation corrections, based on comparisons to the double-spike determined values of *Todt et al.* [1996]. The average fractionation per mass unit was 0.08%.

4. Results and Discussion

4.1. Isotopic Trends With Age: Mauna Loa and Mauna Kea

[14] The HSDP Mauna Loa samples we have measured for He isotopes fill in a gap in the previously studied sample suite between lava classified as old (>150 ka [*Kurz et al.*, 1995]) and young (<$\sim$30 ka [*Kurz and Kammer*, 1991]) (Table 2, Figure 4a). The data in Figure

Table 2. Isotopic Values for Helium and Neodymium Used for Plume Map[a]

Map	Volcano	Age, ka (±30)	Mean R/R_A	R/R_A Range	Mean ε_{Nd}	ε_{Nd} Range
1	Loihi	0	24	5−35	6.1	4.8−8.3
2	Mauna Loa	200	17	16−20	5.5	5.3−5.7
3	Mauna Loa	100	15	14−17	6.0	5.5−6.5
4	Mauna Loa	0	11	8−13	4.5	3.2−7.4
5	Hualalai	0	10	8−16	5.5	5.3−5.7
6	Kilauea	0	16	12−22	6.5	5.9−7.1
7	Mauna Kea	420	11.5	10−13	6.8	6.7−7.2
8	Mauna Kea	300	8[b]	6−8	7.5	7.1−7.7
9	Mauna Kea	200	8[b]		7.4	
10	Mauna Kea	0	8[b]		7.5	6.6−8.5
11	Kohala	240	8[b]		6.6	5.7−7.4
12	Kohala	100	8[b]		7.1	6.8−7.4

[a]Data sources: Loihi [*White and Hofmann*, 1982; *Kaneoka et al.*, 1983; *Kurz et al.*, 1983, *Rison and Craig*, 1983; *Staudigel et al.*, 1984; *Garcia et al.*, 1993; *Garcia et al.*, 1995, 1998]; Mauna Loa [*Kurz and Kammer*, 1991; *Kurz et al.*, 1995; *Lassiter et al.*, 1996; *Abouchami et al.*, 2000; this study]; Hualalai [*O'Nions et al.*, 1977; *Kurz et al.*, 1990]; Kilauea [*O'Nions et al.*, 1977; *Kurz et al.*, 1982, 1983; *Rison and Craig*, 1983; *Hofmann et al.*, 1984; *Newson et al.*, 1986; *Stille et al.*, 1986; *Kurz et al.*, 1987; *Chen et al.*, 1996; *Garcia et al.*, 1996; *Pietruszka et al.*, 1999; *Stracke et al.*, 1999]; Mauna Kea [*Stille et al.*, 1986; *West et al.*, 1988; *Kennedy et al.*, 1991; *Kurz et al.*, 1996; *Lassiter et al.*, 1996]; Kohala [*O'Nions et al.*, 1977; *White and Hofmann*, 1982; *Hofmann et al.*, 1987];

[b]These values are adopted and are nominal. There are no published data except for the circa 300 ka data for Mauna Kea.

4a indicate that the ^{3}He/^{4}He values for Mauna Loa have been gradually declining from values of 17−20 at 200 ka to values of 8−12 in the last 20 ka. This general decrease in ^{3}He/^{4}He values is interrupted by a major excursion to higher values at ∼25−45 ka, and a smaller excursion at 55−75 ka. The typical scatter of values over a 10 kyr window is about ±2 units of Ra, which is relatively small in comparison to the overall shift of 8−10 units over 200 kyr. The trend of decreasing ^{3}He/^{4}He is expected for a plume with a high-He/^{4}He core surrounded by mantle material with ^{3}He/^{4}He values close to those of mid-ocean ridge basalt (MORB, ^{3}He/^{4}He ≈ 8 Ra) [*Kurz et al.*, 1995]. The decrease in ^{3}He/^{4}He correlates with the gradual drift of Mauna Loa away from the plume axis and with a decrease in the eruption rate and lava accumulation rate with time [*Lipman*, 1995]. The gradually changing ^{3}He/^{4}He values contrast with the model favored by *Kurz et al.* [1995], in which the ^{3}He/^{4}He values were argued to change rapidly at ∼30 ka from >15 Ra to values ≤10 Ra. Although this rapid change does occur, the expanded data set shows that it is at the end of

a relatively brief excursion to high ^{3}He/^{4}He, and not representative of the longer-term evolution.

[15] Although the Mauna Loa He isotopic data conform well to a monotonic shift with time, and the shift is in the direction expected, other isotopic systems do not (Figures 4b−4d). The Nd isotopic data (Figure 4b) show a trend of generally increasing ε_{Nd} values from 220 to 20 ka, which is as expected for a volcano moving away from the plume core. However, there is an abrupt shift to lower ε_{Nd} values at ∼20 ka and the low values persist to the present. The Mauna Loa Sr data show relatively little change between 200 and 50 ka, with the exception of a spike toward high ^{87}Sr/^{86}Sr at 50 ka. Starting at 20 ka, the ^{87}Sr/^{86}Sr increased markedly and is generally high to the present. The ^{206}Pb/^{204}Pb values also show relatively little change between 220 and 20 ka, but then change abruptly to lower values.

[16] The isotopic data from Mauna Loa are juxtaposed with the data for the Mauna Kea part of the HSDP core in Figure 5. The Mauna Kea data show a trend of decreasing ^{3}He/^{4}He
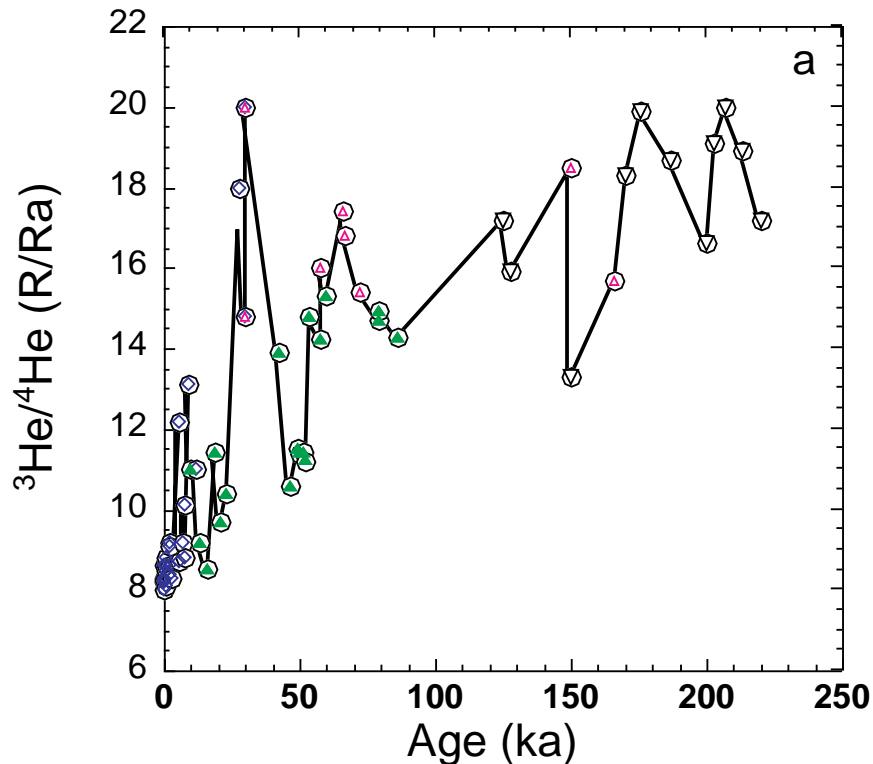
Figure 4. Plots of isotopic ratios versus age for lavas from Mauna Loa. The age assignments are based on geochronology, stratigraphic position, and a model for the lava accumulation rate for Mauna Loa [*DePaolo and Stolper*, 1996]. The ages for the samples older than 100 ka are the most uncertain, but their stratigraphic order is known with certainty. (a) Helium R/Ra versus age. HSDP samples (this study and *Kurz et al.* [1996]) are shown as filled triangles; other data are from the literature (inverted triangle [*Kurz et al.*, 1995], open triangles [*Kurz and Kammer*, 1991] (Kahuku section); open diamonds [*Kurz and Kammer*, 1991]); (b) the neodymium epsilon value versus age; (c) $^{87}Sr/^{86}Sr$ versus age; and (d) $^{206}Pb/^{204}Pb$ versus age.

with time between 430 ka and 200 ka (Figure 5a). Growth models and measured lava accumulation rates, as well as the location of Mauna Kea relative to Mauna Loa, suggest that at ~400–420 ka Mauna Kea was at the stage of evolution corresponding to Mauna Loa at 100–120 ka. The $^3He/^4He$ values of Mauna Kea at 400 ka (10–13 Ra) are lower than the corresponding values for Mauna Loa at 100 ka (14–17 Ra). Given the arrangement depicted in Figure 1, it is evident that Mauna Loa passed almost directly over the center of the plume whereas Mauna Kea passed to the northeast of the plume center. The different $^3He/^4He$ profiles for the two volcanoes are consistent with

Mauna Kea having crossed the plume along a track that was farther away from the plume axis than the track followed by Mauna Loa. Mauna Kea also shows the expected direction of drift of the $^{87}Sr/^{86}Sr$ values, although the shifts are small. The $^{206}Pb/^{204}Pb$ ratio drifts slightly to lower values with time, as does this ratio in the Mauna Loa record.

4.2. Isotopic Maps of the Hawaiian Plume

4.2.1. Construction of the isotopic maps

[17] We now take the analysis of the spatial distribution one step farther by attempting to
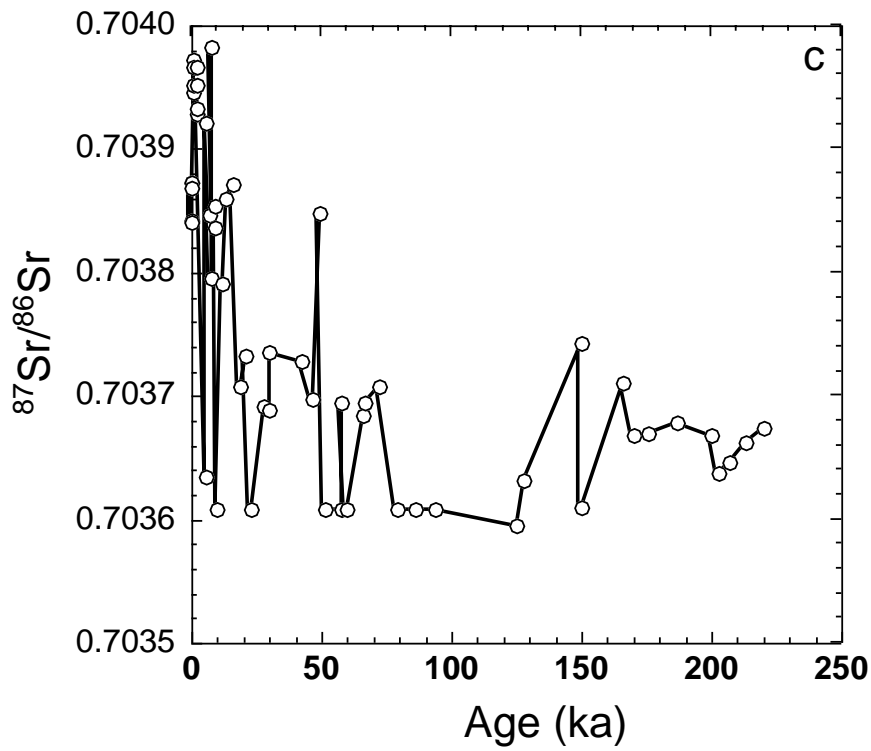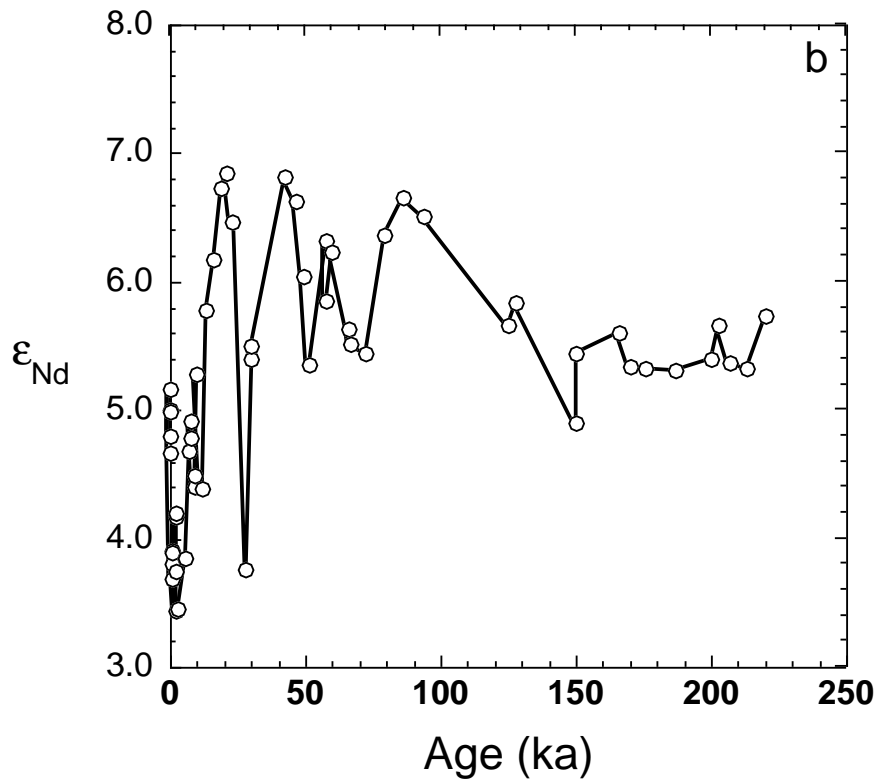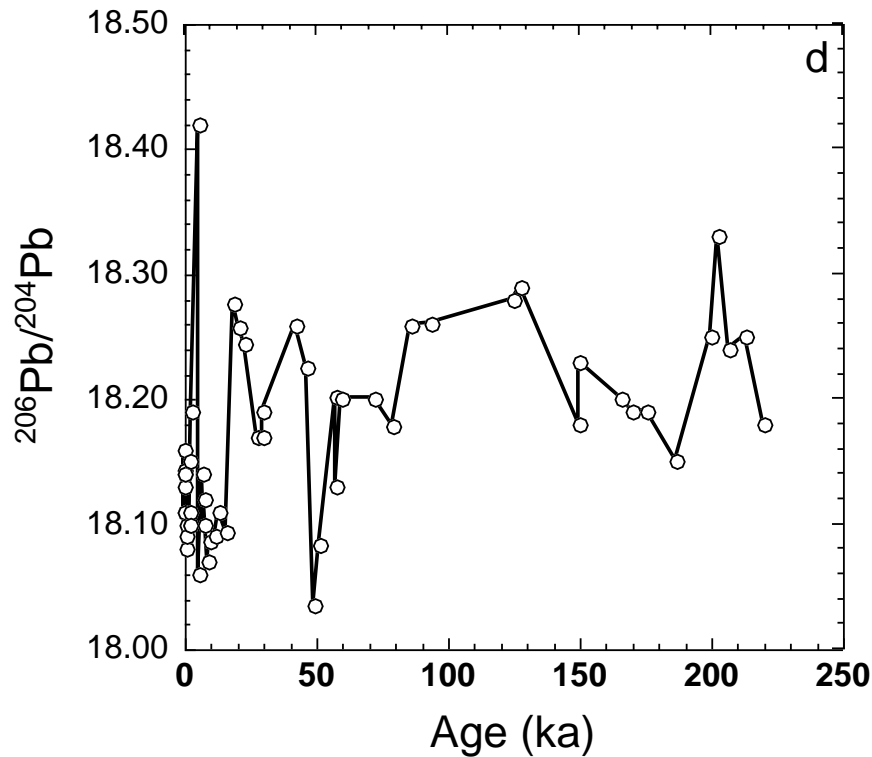
Figure 4. (continued)

Figure 4. (continued)

use the available data to make a map of the isotopic values for He and Nd in the melts coming from the Hawaiian plume. Table 2 summarizes the He and Nd isotopic data for Hawaii and Loihi that we have used from the literature. The observed ranges of $^3He/^4He$ and ε_{Nd} given in the table are keyed to numbered positions shown on Figure 1 along the "track" of each volcano. Many of the data were retrieved using the Mainz GEOROC database (http://GEOROC.MPCH-MAIN-Z.GWDG.DE/). In addition to the data shown in Figures 4 and 5, there are 81 He analyses (Figure 6a) and 182 Nd measurements (Figure 6b). For Kilauea, Loihi, and Hualalai the data are all essentially representative of the present locations of the volcanoes. For the Kohala ε_{Nd} values (there are no published helium data), there is a substantial range of ages represented (~250 kyr).

[18] The data were informally "inverted" for the isotopic distribution in the plume melts. To allow an inversion it is necessary to (1) assign a magma capture area to each volcano, (2) assign concentrations of He and Nd to the melts as a function of the melt supply rate, (3) assign a target level of symmetry for the isotopic distribution. It is also assumed that the spatial distribution of isotopic values in the plume melts is invariant with time over the time span (~400 ka) represented by the data set.

[19] It is assumed that each volcano captures melt from a circular area of radius 25 km centered on the volcano summit. The 25 km radius magma capture area is chosen for consistency with the other parameters in the magma supply model of *DePaolo and Stolper* [1996]. (They used 24 km, but this difference is insignificant for this purpose.) With this choice,
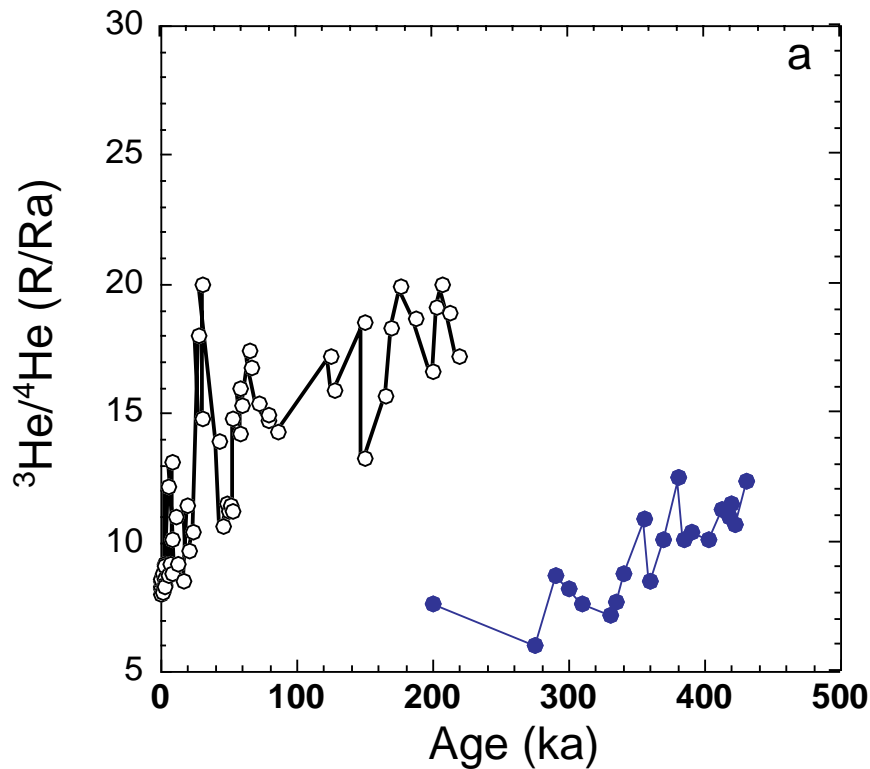
Figure 5. Data from Figure 4 plotted with data for Mauna Kea from the HSDP pilot hole core [*Kurz et al.*, 1996; *Lassiter et al.*, 1996].

the geochemical sampling area is consistent with the magma sampling area needed to grow the volcanoes at the correct rate. Neither the size nor shape of the magma capture area of a volcano or how it might change with the evolution of the volcano and position over the plume, is known from independent evidence or estimable from existing theory. It should be noted that according to the *DePaolo and Stolper* [1996] model, Hualalai, Kohala, and Mauna Kea should not have erupted any lava over the past 200 kyr (Figure 1b). This is more or less correct insofar as the eruption rates on these volcanoes for the past 200 kyr are very small in comparison to the rates for Kilauea and Mauna Loa. For the alkalic phase of these volcanoes we maintain the 25 km magma capture area for the purposes of the inversion and use averages of the isotopic values for many separate eruptive centers. The individual

alkalic vents on these volcanoes probably sample the underlying mantle on a much finer scale. This additional information could be useful for a more detailed analysis of the plume structure, but at present insufficient metadata are available in the literature to fully utilize the existing geochemical data for this purpose.

[20] For the He and Nd concentrations in the plume melts we make the simplifying assumption, valid to first order, that the effective melt fraction is proportional to the melt supply and that the concentration is described by the equilibrium bulk partial melting equations. Hence, in mathematical form

$$c_i(x,y) = c_{io} \left\{ g(x,y)F_{max} + D_i[1 - g(x,y)F_{max}] \right\}^{-1}, \quad (1)$$

where $c_i(x,y)$ is the concentration of element i in melts supplied at location (x,y), F_{max} is the maximum extent of melting in the plume, D_i is
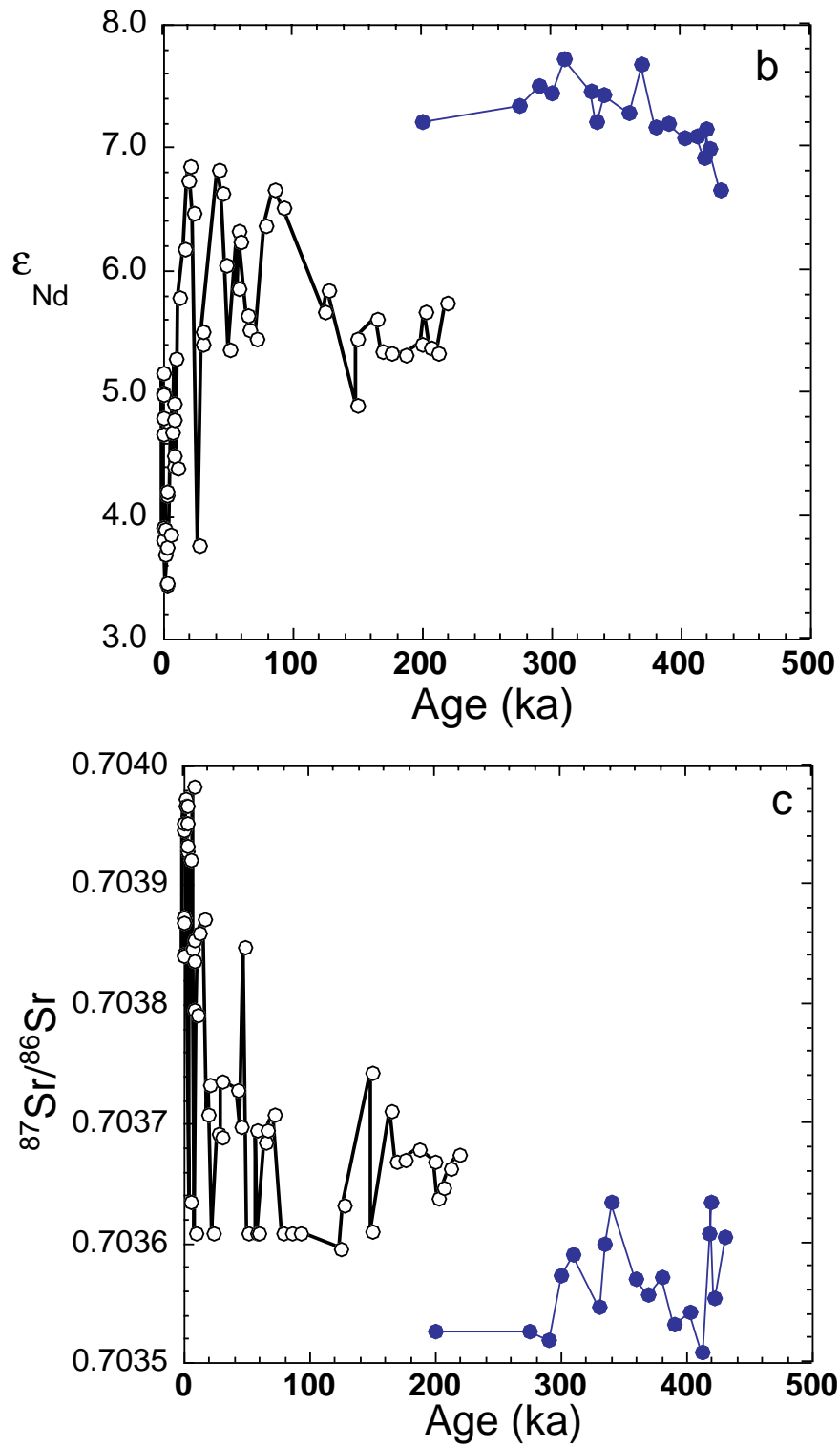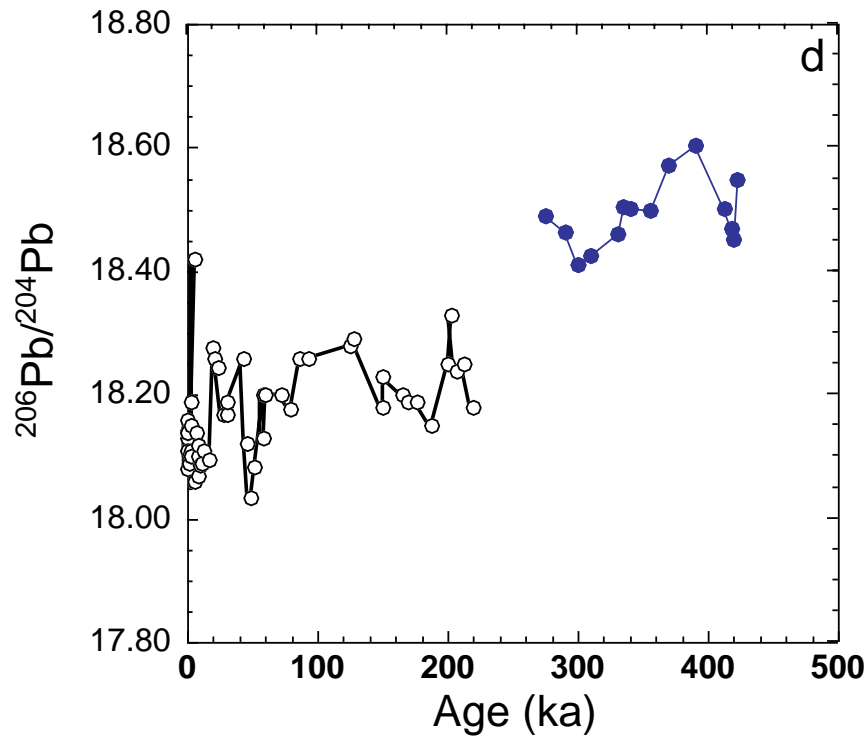
Figure 5. (continued)

Figure 5.   (continued)

the solid/liquid partition coefficient for element i (assumed independent of F), $g(x,y)$ is the melt supply at location (x,y), and c_{io} is a reference concentration.

[21]   The assumption regarding concentration is reasonable to the extent that a steady state melting column produces melts with a concentration that is equal to that of bulk equilibrium melting [*Spiegelman and Elliott*, 1993] and that there must be some correlation between melt fraction and melt supply. The unknown is whether there are variations in the elemental concentrations in the solid mantle source material, and whether such concentration variations correlate with isotopic composition. For a highly incompatible element (which probably applies to helium), Equation (1) makes the concentration proportional to the inverse of melt supply. When the contributions of melts

from different areas of the plume are weighted by melt supply, the result is that there is no spatial weighting factor, since the variations in melt supply cancel the variations in melt fraction. For less incompatible elements like Nd or compatible elements like Os, the spatial weighting factors can be as variable as the melt supply. For Nd we have assumed that the minimum melt fraction is 1% (far from the plume core), which is roughly compatible with measured Nd concentrations in silica-undersaturated lavas. The result is that the spatial weighting factors for Nd isotopes vary by a factor of 4.6 between the far field and plume core. The inversion was done with and without the spatial weighting factors to evaluate their effect.

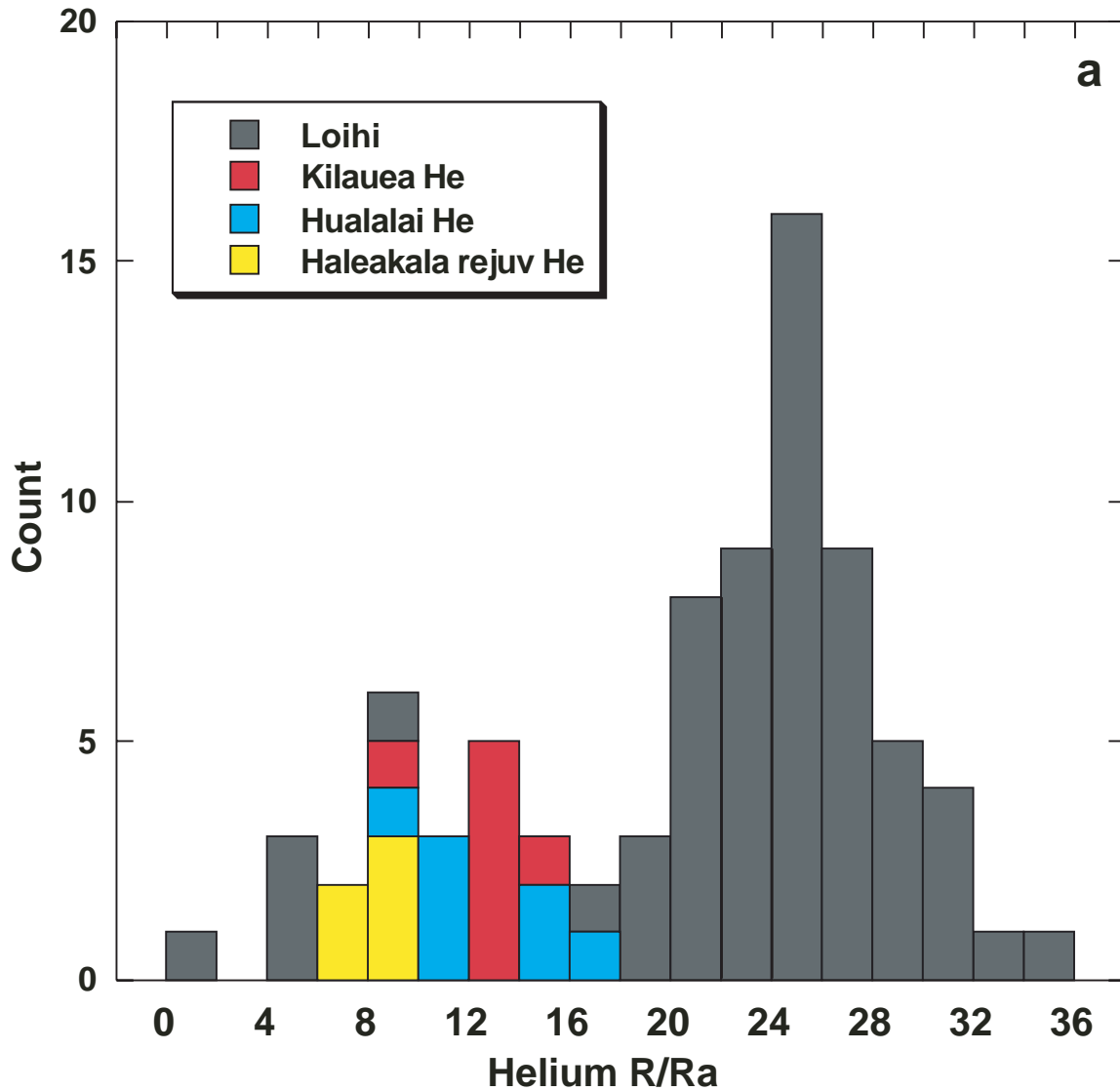[22]   The starting point for the inversion is an isotopic distribution that mimics the melt sup-

Figure 6. Histograms of other Hawaiian data used in construction of isotope maps: (a) Distribution of He data and (b) distribution of Nd data. Data compilation facilitated by the GEOROC database. Sources for the data used in the histograms and in the figures are given in Table 2.

ply pattern of *Ribe and Christensen* [1999] in that it is symmetric about the ridge axis, has the extreme plume values coincident with the maximum in melt supply, and approaches radial symmetry on the upstream (southeast) side of the plume. This starting distribution corresponds approximately to having the isotopic values correlate with plume temperature (and

upwelling rate), which should be roughly true if the plume consists mainly of deeply derived hot material that has entrained cooler and geochemically different mantle material on its way upward. This simple picture is only the starting distribution. If the starting distribution were an accurate representation of the plume structure, then it should fit the observations with little
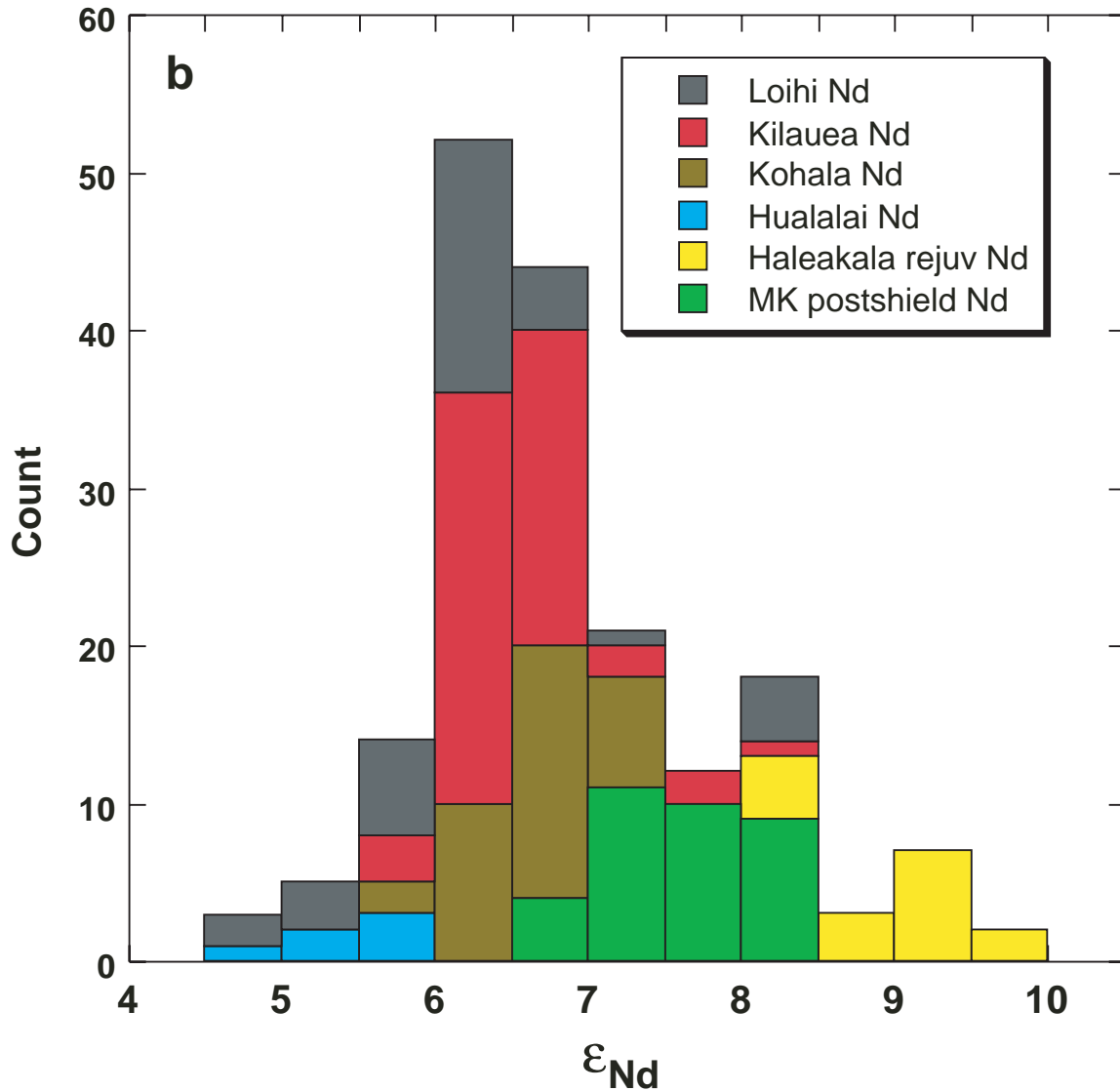
Figure 6. (continued)

modification. However, substantial modification is necessary as shown below. An alternative starting distribution could equally well have been used (for example, a radially symmetric model). The data could also be fit with a model that has much less symmetry, since the capture areas of the different volcanoes do not overlap in many areas. The results we present can be considered as best fits for models that preserve radial symmetry near the plume core and transverse symmetry northwest of the plume core.

[23] The data were "fit" iteratively. The distribution of $^3He/^4He$ and ε_{Nd} values in the plume melts were distributed on a 10 km grid, extending to 100 km either side of the plume track, 100 km upstream, and 200 km downstream (to

the northeast) of the point showing the peak magma supply in Figure 1a. The distribution of the isotopic parameters was gradually modified from the original guess to fit the values for the volcanoes while maintaining as much of the original symmetry as possible. There were two considerations in establishing a ''good fit.'' The average value of $^3He/^4He$ and ε_{Nd} for each volcano (at each position) needed to be matched, but also the range of values displayed at each position must be accessible within the 25 km radius melt capture area of the volcano. The resulting fit gives the average volcano values to within ± 1 unit of Ra and ± 0.2 units of ε_{Nd}.
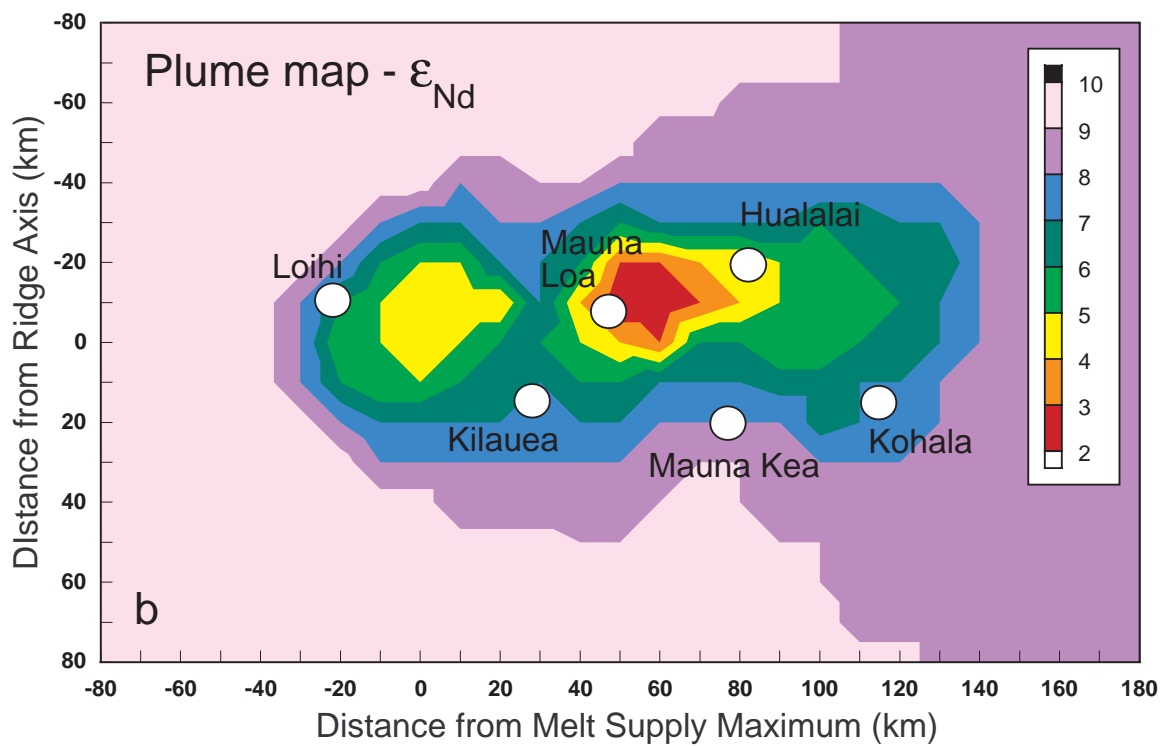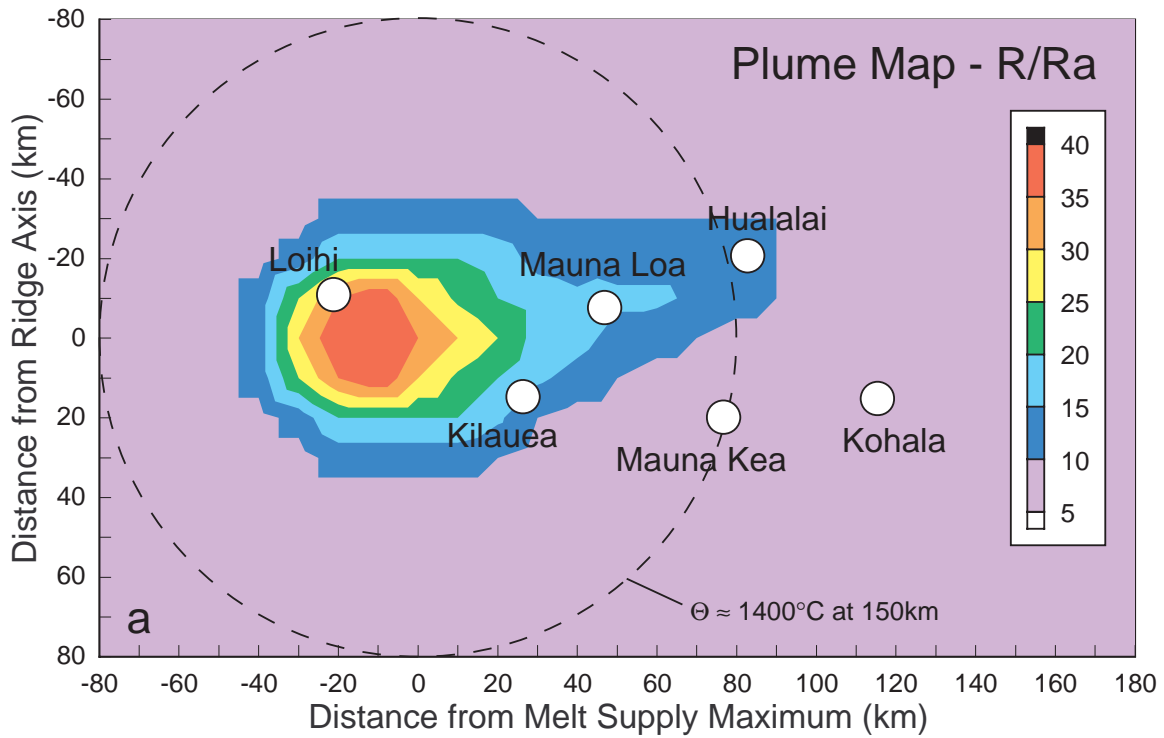
[24] The results of the inversion are shown in Figures 7 and 8. Figure 7 shows the values inferred for the plume melts. Figure 8 shows the average value of the lavas erupting from a volcano as a function of the position of the volcano summit. The quality of the model fit can be assessed by comparing Figures 8a and 8b with the numbers in Table 2 and the data in Figures 4 and 5. For example, the average value for $^3He/^4He$ for Loihi can be read from Figure 8a as being ~ 23 Ra, and the value given in Table 2 is 24 Ra. The average value for ε_{Nd} for Kilauea is 6.5 from Figure 8b and 6.5 from Table 2. The average values used for Mauna Loa and Mauna Kea are derived from the data shown in Figure 5 using ± 50 ka windows. The sharp changes in isotopic composition shown by the Mauna Loa lavas of the past 20 to 30 kyr cannot be accurately reproduced by this model. The spatial averaging over the magma capture area does not allow for such sudden changes. Hence it may be inferred that such sudden changes result from preferential sampling within the magma capture area, the location of the magma source changing rapidly with time. The use of spatial weighting factors affects the Nd isotope maps only in the region near the highest melt supply. The effect of the weighting factor is to decrease the amplitude of

the Nd isotopic anomaly associated with the plume core. With the weighting factors a value of $\varepsilon_{Nd} = 4$ in the plume core is sufficient to account for the Loihi data. Without the weighting factors, a value closer to $\varepsilon_{Nd} = 3$ is necessary.

4.2.2. Plume isotopic structure and components

[25] In large measure the He data (Figures 7a and 8a) can be accommodated with a concentric plume with a high $^3He/^4He$ core (maximum value of ~ 40 Ra) grading outward to ambient mantle material with $^3He/^4He$ of 8 Ra. The contours are approximately circular, except on the downstream (northwest) side of the plume, where the $^3He/^4He = 10$ Ra contour is required to extend farther from the plume axis to capture the relatively high values found in Hualalai and some Mauna Loa samples. This departure from axisymmetry is broadly consistent with the flow of the plume under the moving lithosphere. The large range in values, for both $^3He/^4He$ and ε_{Nd}, at Loihi implies that the contours are closer together near Loihi than elsewhere, and that the radius of the plume isotopic signal is less than the 50 km width of the magma capture area. Relatively close contours are expected for the upstream side of the plume where the northwestward mantle flow compresses the plume (cf. Figure 1 and *Ribe and Christensen* [1994, 1999]). The fact that Loihi is erupting alkalic as well as tholeiitic basalts also indicates that it is near the edge of the plume melting region. The plume He isotopic signal presumably does not persist downstream much farther than the present location of Hualalai. The $^3He/^4He$ values higher than 20 Ra appear to be restricted to the region between Kilauea and Loihi.

[26] The Nd isotopic map of the plume (Figure 7b) shows some similarities and differences with the He map (Figure 7a). Although the
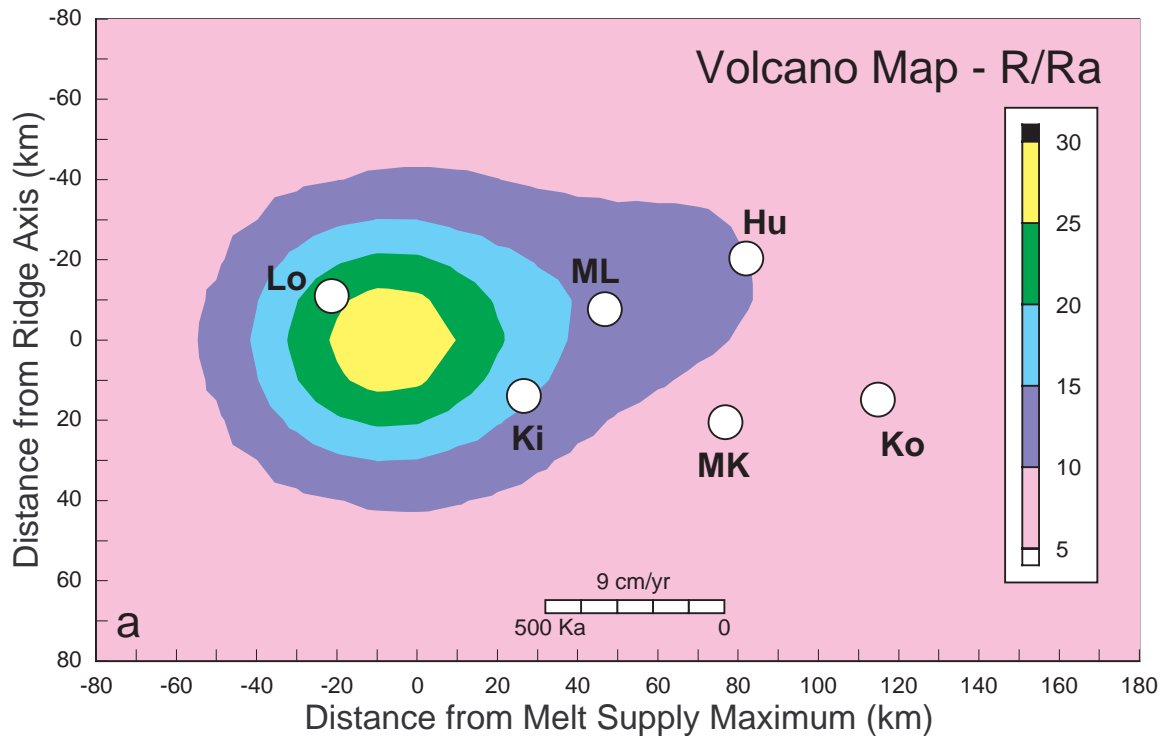
Figure 8. (a) Map of model average volcano $^3He/^4He$ values as a function of the location of the volcano summit (the center of its magma capture area). (b) Map of average volcano ε_{Nd} values. These maps can be used to evaluate the fit of the plume model (Figure 7) to the data in Table 2 and Figure 1.

Nd data allow for a pattern approaching concentric isopleths between Kilauea and Loihi, the data require a long, low-ε_{Nd} tail extending toward Hualalai. This tail is depicted in Figure 6b as being interrupted between Mauna Loa and Kilauea by a high-ε_{Nd} ridge. The ridge is needed to account for the high ε_{Nd} values for Mauna Loa samples with 100–30 kyr ages (Figure 5b). The data also require a large "blob" of particularly low-ε_{Nd} material located

between Mauna Loa and Hualalai. The ε_{Nd} values in this blob appear to be more extreme than the values required to fit the main plume core between Kilauea and Loihi. A similar pattern would be needed for the Sr isotopes, which roughly correlate with Nd. The Nd isotopic tail extends in the same direction as that for He but is more intense and extends much farther. There is no constraint at present on how far the low-ε_{Nd} tail extends beyond the

Figure 7. (a) Deduced distribution of helium $^3He/^4He$ values in melts coming from the Hawaiian plume. This distribution results in average values for the lavas from each volcano as depicted in Figure 8a. It is assumed that each volcano samples a circular area of the plume with radius 25 km, centered on the volcano summit, and that the He contribution is proportional to area sampled rather than melt production rate, which should apply for incompatible elements. The line $y = 0$ on this map would correspond to the axis of the Hawaiian Ridge [Moore, 1987] as defined by seismic refraction data and would have a bearing of N30°W. (b) Deduced distribution of ε_{Nd} values in melts coming from the Hawaiian plume.
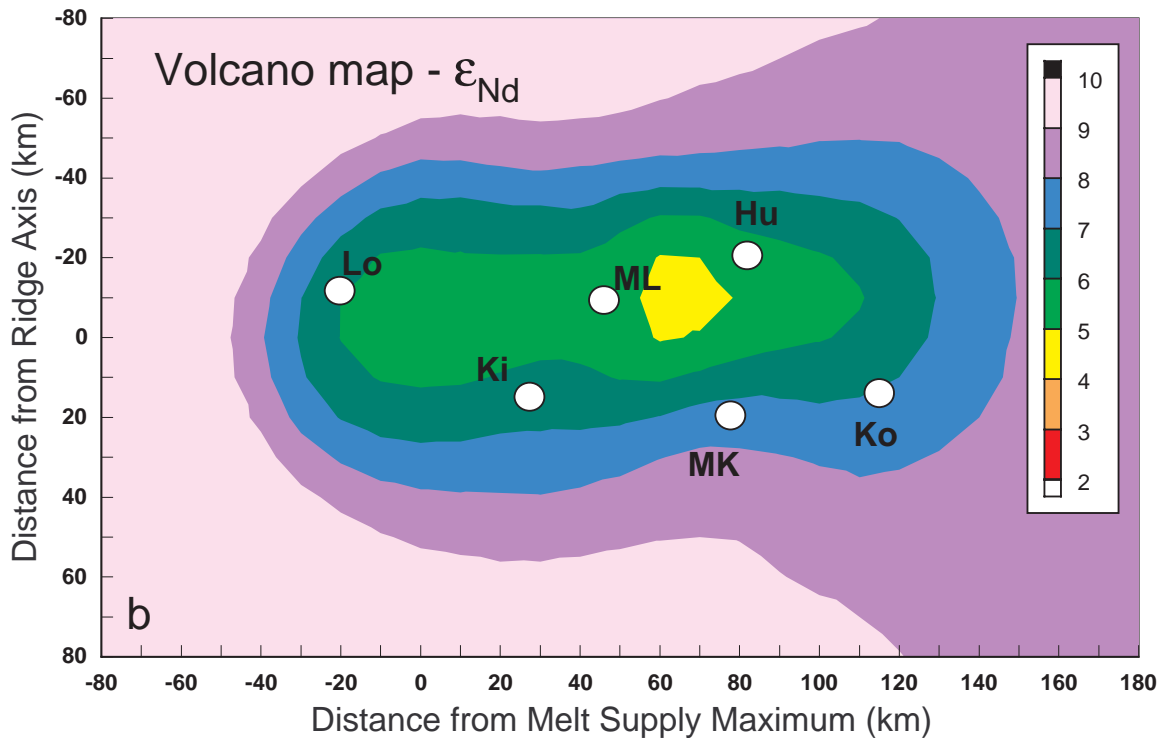
Figure 8.   (continued)

magma capture area of Hualalai. As noted above, the high measured values of the Mauna Loa 50–100 ka samples are not accurately captured by the model shown in Figures 7a and 7b, because the isotopic shifts are too abrupt and of too large a magnitude. If these high values were not taken into account, there would be a continuous, low-ε_{Nd} trough extending from the plume core to Hualalai. The inclusion of the recent Mauna Loa data produces the requirements for the low-ε_{Nd} anomaly between Mauna Loa and Hualalai.

[27] Superimposed on the plume He isotope map (Figure 7a) is a circle of radius 80 km, which corresponds roughly to the radius of the plume at a potential temperature, $\Theta = 1400°C$, at a depth of 140–150 km in the *Ribe and Christensen* [1999] model. At this depth, which corresponds to the deepest levels of melting in

the hot core, the plume is already spreading due to the interference of the lithosphere lid. The corresponding plume radius at 170 km depth is ~60 km. The 1400°C potential temperature is still well above the ambient mantle potential temperature of 1300°C. The isotopic map shows that the strong isotopic signatures of the plume ($^3He/^4He$ >15 Ra and ε_{Nd} < 6), are confined to the hot core of the plume. This isotopically distinct plume core has a radius of ~20–25 km and corresponds (in the Ribe and Christensen model) to potential temperatures in excess of 1565°C (~90% of the maximum excess temperature). The narrowness of the isotopic anomaly and its association with only the highest Θ values confirms that the plume signature comes from deep in the mantle and that the material with this signature makes up only a small percentage of the total volume of upwelling mantle.

[28]   The Nd isotope map of the plume (Figure 7b) depicts a subtle plume influence spreading downstream to more than 80 km to either side of the Hawaiian Ridge. This feature is only schematic as there are no constraints outside the volcano magma capture areas. Historical lavas from Haleakala show a very weak plume signature ($\varepsilon_{Nd} \approx 9$), indicating that the plume is highly attenuated at that position. However, it has also been inferred that lavas dredged from the North Hawaiian Arch, far off the ridge axis, have ε_{Nd} and $^{87}Sr/^{86}Sr$ values that have a slight plume influence.

[29]   The highest $^3He/^4He$ values occur centered about a point that is displaced $\sim 10-15$ km upstream (toward the southeast) from the location of the peak magma supply from the plume. This displacement, which is required by the high $^3He/^4He$ values of Loihi, has been noticed previously and attributed to the nonverticality of the plume [Kurz et al., 1996]. For the Ribe and Christensen model the location of the peak eruption rate for each volcano is displaced downstream from the magma supply maximum by another 10 km due to the asymmetry of the melt supply contours. Hence the peak $^3He/^4He$ values are displaced 20–25 km upstream from the point that would correspond to the peak volcano growth rate. For a plate velocity of 9 cm/yr this implies that the highest $^3He/^4He$ values occur in each volcano ~ 250 kyr prior to the peak eruption rates. Because the ε_{Nd} contours are drawn out in the downstream direction, it is more difficult to locate the point for ε_{Nd} that corresponds to the $^3He/^4He$ maximum, but it appears from Figure 7b that it may be coincident with the $^3He/^4He$ maximum, or slightly farther downstream (to the northwest).

[30]   The $^3He/^4He = 20$ Ra contour of the plume melts appears to be closed, reaching only about as far as the summit of Kilauea in the downstream direction. This implies that the He isotopic anomaly resides in a narrow zone at the plume core and that the plume isotopic signature is removed in the early stages of melting. The material that passes through the melting region in the plume core and is then advected downstream by the lithosphere drag [cf. Ribe and Christensen, 1999, Figure 5], is therefore mostly devoid of its original helium and does not significantly influence the helium isotopic composition of the melts near the present locations of Mauna Loa, Hualalai and Mauna Kea. This observation requires that helium behave as a strongly incompatible element, with a K_D of ~ 0.001 or less, so that it is almost quantitatively removed from the mantle source material by the time the melt fraction reaches a few percent. The fact that the Nd isotopic contours (also Sr) extend farther downstream is expected. The Nd in the magma source material is reduced to 10% of original concentration only when the melt fraction reaches about 0.16 (assuming K_D is 0.023). The Ribe and Christensen [1999] model shows that such high melt fractions are reached only downstream (under Mauna Loa) and that they do not exceed 0.16 by very much. Hence it is expected, as observed, that the Nd isotopic plume signature would be present for an extended distance downstream.

[31]   The low ε_{Nd} values in the Mauna Loa–Hualalai region apparently reflect a bloblike heterogeneity in the plume that has a length scale of circa 20 km (after having been stretched out by the flow under the lithosphere). This low-ε_{Nd} region between Mauna Loa and Hualalai cannot be a continuous ring as suggested by Rhodes and Hart [1995] and Hauri et al. [1996], because that possibility is precluded by the HSDP Mauna Kea data (Figures 1 and 5). The Mauna Loa–Hualalai blob is not apparent in the He isotope data. This discrepancy can be interpreted in two ways. Either this blob is different from the plume core in that low-ε_{Nd} is not associated with high $^3He/^4He$ or this part of the plume has been
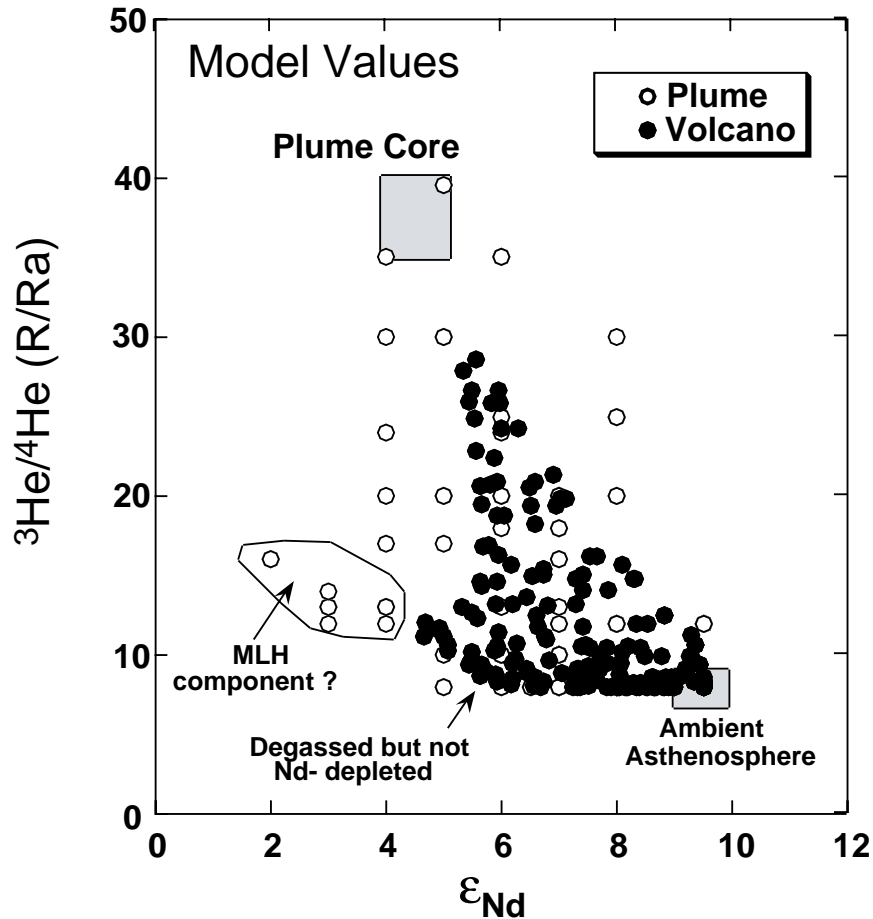
Figure 9. Relationship between helium $^3He/^4He$ and ε_{Nd} value for average volcano products (solid symbols) and plume melts (open symbols) based on the maps of Figures 7 and 8. Early degassing of high $^3He/^4He$ helium from the plume core results in a decoupling of the He signal from that of the less incompatible element Nd. Lavas erupted from volcanoes located downstream of the plume core epicenter thus typically have plume signatures for Nd but little or no plume signature for He. The "degassed but not Nd-depleted" material in the plume will appear to be a different plume component but was actually generated by the melting process in the plume and may not reflect material present in the mantle prior to melting. The designation "MLH component" (for Mauna Loa–Hualalai) represents the region of the plume map (Figure 7) between Mauna Loa and Hualalai. This material may also be affected by degassing of helium.

previously stripped of He by partial melting nearer the plume core but still retains its Nd isotopic signature.

[32] The difference of incompatibility between He and Nd (and Sr, Pb, etc.) is important for assessing the overall patterns in the isotope-isotope plots of Hawaiian lavas. The type of pattern expected is illustrated in Figure 9, which is another representation of the information in the maps of Figures 7 and 8. Assuming the plume has a well-defined composition for $^3He/^4He$ and ε_{Nd}, the resulting lavas do not lie along a single mixing trajectory. Instead, they fill in a substantial area on the graph. This may be the explanation for the distribution of data

on the various plots of ^{3}He/^{4}He versus another, less incompatible, element's isotope ratio (Sr, Nd, Hf) [e.g., *Kurz and Kammer*, 1991; *Kurz et al.*, 1995]. The solid points in the graph represent compositions averaged over the volcano magma capture areas (Figure 8), whereas the open symbols represent the actual, somewhat larger, distribution in the melts available from the plume (Figure 7).

[33] There are a number of other general statements that can be made based on the isotopic maps. One important point, previously made by *DePaolo and Stolper* [1996], is that the full magnitude of any isotopic anomaly is not likely to be exhibited by the volcanic products due to the spatial averaging associated with the size of the magma capture region. Hence, although the plume map requires regions with ^{3}He/^{4}He values of 40 Ra and ε_{Nd} values as low as about +2, the volcanic products are unlikely to exhibit values higher than about ^{3}He/^{4}He = 30 Ra or lower than ε_{Nd} = +4.5. The most extreme values measured are therefore only limits on the values in the plume core. The values shown in the plume map (Figure 7) were chosen so as to minimize the amplitude of the isotopic anomaly associated with the plume core. The lava values (Figure 8) are not sensitive to the presence of a small inner plume core with extreme isotopic values. The isotopic variations of the volcanoes as a function of time are also expected to be rather subdued for the moderately incompatible elements. As shown in Figure 8b, for Nd the variations of ε_{Nd} with time for the Kea trend volcanoes is small because they are following ε_{Nd} contours. The Loa trend volcanoes such as Hualalai may also show very small variations over most of their eruptive history due to the downstream advection of the isotopic anomalies. Only the early stages of each volcano are likely to be isotopically highly variable because the isotopic variations become more subdued due to the combined effects of melting and spreading of the plume

material in the downstream direction. For highly incompatible elements like He, larger variations with time are to be expected (and are observed), even in the downstream region of the plume.

4.2.3. Plate and plume motions

[34] The reconstruction of the volcano summit positions with age (Figure 1) was done assuming plate motion relative to the plume in the direction N30°W. The basis for this is that the seismically defined axis of the ridge (Figure 10, adapted from *Moore* [1987]) lies along this trend between Maui and Loihi. Even without the seismic data, a trend close to N30°W would be deduced by connecting the midpoint of the ridge at Maui with the midpoint of the ridge at Kilauea. Using this trend, all of the volcanoes of Hawaii can be inferred to have passed within reasonable proximity of the plume axis. Hence the inference that the plate has been moving along a trend of N30°W relative to the plume for the past 1.5–2 million years seems reasonable, and it is also consistent with the proposal by *Wessel and Kroenke* [1997] based on their "hot spotting" technique.

[35] Relative to the Hawaiian Ridge axis the extension of the ^{3}He/^{4}He = 10 Ra contour is displaced to the southwest (toward Hualalai and away from Mauna Kea; Figure 7a). Whereas the trend of the Hawaiian Ridge is approximately N30°W, the axis of the ^{3}He/^{4}He pattern lies along a trend of approximately N40°W. A more westerly trend for the isotopic tail is allowed because there are poor constraints on the structure of the southwest side of the plume. The trend of neither the axis of the Hawaiian Ridge between Maui and Loihi, nor the ^{3}He/^{4}He pattern matches the direction of modern plate motion measured by Laser Ranging GPS, which averages N63°W for four stations located on Hawaii and Maui (http://sideshow.jpl.nasa.gov/mbh/series.html). The
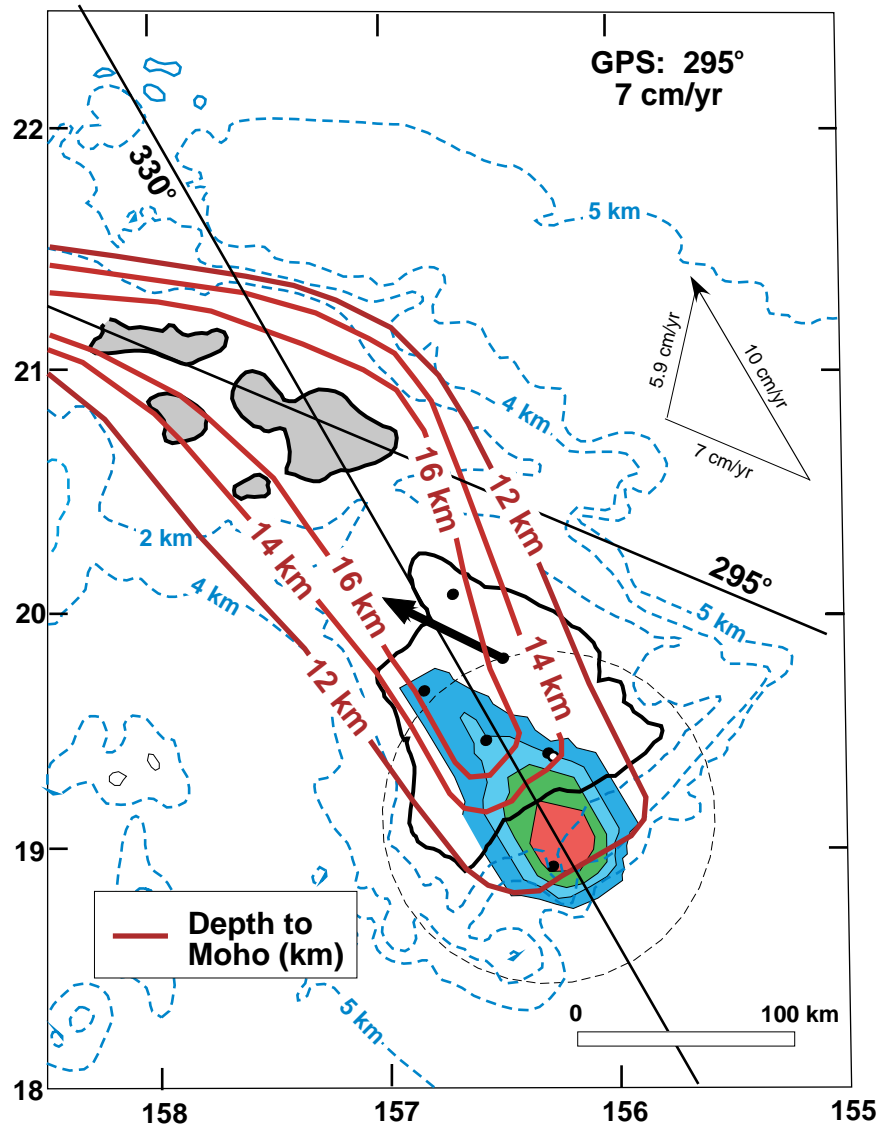
Figure 10. Plate and plume motions in Hawaii. Bathymetry data in dashed blue lines. The red contours are the seismically defined ridge axis [after *Moore*, 1987]. Recent GPS measurements (http://sideshow.jp.lnasa.gov/mbh/series.html) yield an absolute plate velocity of 7 cm/yr in the direction of N63°W, similar to the N65°W trend of the Hawaiian swell. One way to reconcile the modern GPS measurements with estimates of long-term Pacific plate velocity is to have the plume migrating SSW at a velocity of ca. 6 cm/yr (see text for discussion). Superimposed upon the geophysical data is the He map of the Hawaiian plume (Figure 7a). Note the orientation of the axis of the He pattern lies N40°W, off the axis of the trend of the Hawaiian Ridge (N30°W).

GPS vector is quite close to the long-term trend of the Hawaiian Ridge between Hawaii and Midway (N65°W), and to the trend inferred for the axis of the Hawaiian swell.

[36] The velocity of the Pacific plate relative to the plume is also an issue. The GPS results suggest an absolute plate velocity of 7 cm/yr. The age progression in the Hawaiian chain

overall suggests a long-term relative velocity of about 8 to 9 cm/yr. *Moore and Clague* [1992] have suggested that the modern relative velocity might be as high as 13 cm/yr. Assuming that the GPS value is meaningful and representative of more than just a present-day transient, a possible explanation of the discrepancies is that the plume is moving to the south or southwest. For example, if the plume has been moving southward along a trend of N13°E at a velocity of 5.9 cm/yr for the past 1.5 million years, then the resultant velocity of the plate relative to the plume would be 10 cm/yr along a trend of N30°W (Figure 10). The change in the trend of the Hawaiian Ridge at Maui may require such motion.

[37] There are insufficient data to determine the precise value of the plate velocity relative to the plume for the past 1 or 2 million years. Geochronological constraints are not tight enough because the ages available for the older volcanoes (e.g., Kohala) are not tied closely enough to the volcano growth stage. The limited geochronological data on Mauna Kea lavas from the HSDP Pilot Hole suggest that a velocity in the neighborhood of 10 cm/yr is appropriate [*DePaolo and Stolper*, 1996]. Both the trends of the volcano tracks shown in Figure 1, and the resultant isotopic maps (Figures 7 and 8) are subject to the uncertainties in the velocity and direction of motion. Changing the relative plume-plate velocity by ±1 cm/yr will not significantly alter the isotopic maps. However, changing the trend of the motion from N30°W to N65°W would drastically alter the results, and make it difficult to make any model to explain the location and volumes of the volcanoes of the island of Hawaii.

5. Summary and Conclusions

[38] New He isotopic data from the HSDP pilot hole core, lava accumulation rate models, and data from the literature have been used to develop a 200,000 year isotopic record for the lava erupted from the Mauna Loa volcano. This record, an analogous record from Mauna Kea derived from the HSDP pilot hole project, and other literature data on Hawaiian volcanoes from the GEOROC database, have been used to construct a "map" of lava isotopic compositions for the island of Hawaii. The isotopic map takes account of the drift of the volcanoes over the plume magma sources with time assuming that the Pacific plate velocity is 9 cm/yr relative to the plume along a trend of N30°W.

[39] The isotopic map of Hawaii has been converted to a map of the isotopic compositions of melts arriving at the top of the plume melting region, for the elements He and Nd. This inversion was done informally. The initial assumption was that the isotopic structure of the plume mimics the melt production map developed by *Ribe and Christensen* [1999] from their geodynamic model of the Hawaiian plume. This approach tends to maximize radial geochemical structure for the plume. The plume melt isotopic values, arranged on a fairly coarse 10×10 km grid, were then adjusted until the average isotopic values of the volcanoes were matched to within about 1 unit of R/Ra for He and 0.2 units of ε_{Nd}. In calculating the isotopic compositions of the volcanic products, it was assumed that each volcano captures magma from, and averages, melts from the plume over a circular area of radius 25 km centered on the volcano summit. This magma capture area model is consistent with the growth rates and total volumes of Hawaiian volcanoes to the extent that this can be tested at present [*DePaolo and Stolper*, 1996].

[40] The resulting map of the plume has several important features. Helium isotopes can be accounted for with an axisymmetric model. The high-^{3}He/^{4}He part of the plume (R/Ra > 20) is confined to a zone of radius 20–25 km at

the core of the plume. In the *Ribe and Christensen* [1999] model, this part of the plume has a high potential temperature (>1565°C), more than 90% of the maximum temperature anomaly in the plume relative to the ambient mantle. This suggests that the He isotopic signal is derived from very deep in the mantle. The $^3He/^4He$ map has closed contours down to $^3He/^4He$ = 10 Ra, although the contours are teardrop-shaped, being elongated in the direction of Pacific plate motion. The direction of elongation of the contours is not precisely on the Hawaiian ridge axis. The closed contours indicate that the plume He signal is thoroughly lost during the early stages of melting, which is consistent with helium behaving as a strongly incompatible element ($K_{He} \leq 0.001$). Nd isotopes are also broadly consistent with axisymmetric geochemical structure. As with helium, the low-ε_{Nd} part of the plume (values <6) is confined to the inner core of the plume. However, the ε_{Nd} contours do not all close on the scale of the island of Hawaii but instead follow material flow lines within the plume and hence tend to be nearly parallel to the ridge axis for a substantial distance in the direction of plate motion. This is consistent with the moderately incompatible behavior of Nd ($K_{Nd} \approx 0.02$). One result of the difference in behavior of the highly incompatible He and the less incompatible Nd (also Sr, Pb, Hf, Os) is that downstream from the plume core epicenter the lavas tend to have plume isotopic signatures for the less incompatibles, but asthenospheric signatures for He. These characteristics could be mistaken for an additional plume component [*Lassiter et al.*, 1996; *Kurz et al.*, 1996].

[41] A low-$^3He/^4He$ plume component that has low ε_{Nd} and high $^{87}Sr/^{86}Sr$ is evident only in recent Mauna Loa lavas (ages <20 ka for the most part). The plume map suggests that this low ε_{Nd}, high $^{87}Sr/^{86}Sr$ component may constitute a blob located between Mauna Loa and Hualalai and that this blob is separated from the main plume core by a zone of more asthenosphere-like material with high ε_{Nd} and low $^{87}Sr/^{86}Sr$. The low-$^3He/^4He$ values could be due to previous degassing of this blob near the plume core at depth, rather than signifying a separate plume component.

Acknowledgments

References

Abouchami, W., S. J. G. Galer, and A. W. Hofmann, High precision lead isotope systematics of lavas from the Hawaiian Scientific Drilling Project, *Chem. Geol.*, *169*, 187–209, 2000.

Baker, M. B., S. Alves, and E. M. Stolper, Petrography and petrology of the Hawaii Scientific Drilling Project lavas: Inferences from olivine phenocryst abundances and compositions, *J. Geophys. Res.*, *101*, 11,715–11,727, 1996.

Beeson, M. H., D. A. Clague, and J. P. Lockwood, Origin and depositional environment of clastic deposits in the Hilo drill hole, Hawaii, *J. Geophys. Res.*, *101*, 11,617–11,629, 1996.

Chen, C.-Y., F. A. Frey, J. M. Rhodes, and R. M. Easton, Temporal geochemical Evolution of Kilauea volcano: Comparison of Hilina and Puna basalt, in *Reading the Isotopic Code, Geophys. Monogr. Ser.*, vol. 95, edited by A. Basu and S. Hart, pp. 161–181, AGU, Washington, D. C., 1996.

Clague, D. A., The growth and subsidence of the Hawaiian-Emperor volcanic chain, in *The Origin and Evolution of Pacific Island Biotas, New Guinea to Eastern Polynesia: Patterns and Processes*, edited by A. Keast and S. E. Miller, pp. 35–50, Academic, San Diego, Calif., 1996.

DePaolo, D. J., Study of magma sources, mantle structure and the differentiation of the earth using variations of ^{143}Nd/^{144}Nd in igneous rocks, Ph.D. dissertation, 360 pp., Calif. Inst. of Technol., Pasadena, 1978.

DePaolo, D. J., and E. M. Stolper, Models of Hawaiian volcano growth and plume structure: Implications of results from the Hawaii Scientific Drilling Project, *J. Geophys. Res.*, *101*, 11,643–11,654, 1996.

Dodson, A., D. J. DePaolo, and B. M. Kennedy, Helium isotopes in lithospheric mantle: Evidence from Tertiary basalts of the western USA, *Geochim. Cosmochim. Acta*, *62*, 3775–3787, 1998.

Frey, F. A., and J. M. Rhodes, Intershield geochemical differences among Hawaiian volcanoes: Implications for source compositions, melting processes and magma ascent paths, *Philos. Trans. R. Soc. London*, *352*, 121–136, 1993.

Garcia, M. O., B. A. Jorgenson, J. J. Mahoney, E. Ito, and A. J. Irvina, An evaluation of temporal geochemical evolution of Loihi summit lavas—Results from Alvin submersible dives, *J. Geophys. Res.*, *98*, 537–550, 1993.

Garcia, M. O., D. J. P. Foss, H. B. West, and J. J. Mahoney, Geochemical and isotopic evolution of Loihi Volcano, *Hawaii, J. Petrol.*, *36*, 1647–1674, 1995.

Garcia, M. O., J. M. Rhodes, F. A. Trusdell, and A. J. Pietruszka, Petrology of lavas from the Puu Oo eruption of Kilauea Volcano, 3, The Kupaianaha episode (1986–1992), *Bull. Volcanol.*, *58*, 359–379, 1996.

Garcia, M. O., K. H. Rubin, M. D. Norman, J. M. Rhodes, D. W. Graham, D. W. Muenow, and K. J. Spencer, Petrology and geochronology of basalt breccia from the 1996 earthquake swarm of Loihi Seamount, Hawaii; magmatic history of its 1996 eruption, *Bull. Volcanol.*, *59*, 577–592, 1998.

Geist, D., W. White, T. Naumann, and R. Reynolds, Illegitimate magmas of the Galapagos: Insights into mantle mixing and magma transport, *Geology*, *27*, 1103–1106, 1999.

Getty, S. J., and D. J. DePaolo, Quaternary geochronology by the U-Th-Pb method, *Geochim. Cosmochim. Acta*, *59*, 3267–3272, 1995.

Hauri, E. H., J. A. Whitehead, and S. R. Hart, Fluid dynamic and geochemical aspects of entrainment in mantle plumes, *J. Geophys. Res.*, *99*, 24,275–24,300, 1994.

Hauri, E. H., J. C. Lassiter, D. J. DePaolo, and J. M. Rhodes, Osmium isotope systematics of drilled lavas from Mauna Loa, Hawaii, *J. Geophys. Res.*, *101*, 11,793–11,806, 1996.

Herzberg, C., P. Raterron, and J. Zhang, New experimental observations on the anhydrous solidus for peridotite KLB-1, *Geochem. Geophys. Geosyst.*, *1*, Paper number 2000GC000089 [4498 words, 7 figures, 4 tables], 2000.

(Available at http://www.g-cubed.org/publicationsfinal/databriefs/2000GC000089/fs2000GC000089.html)

Hirschmann, M. M., Mantle solidus: Experimental constraints and the effects of peridotite composition, *Geochem. Geophys. Geosyst.*, *1*, Paper number 2000GC000070 [11,012 words, 12 figures, 3 tables], 2000. (Available at http://www.g-cubed.org/publicationsfinal/articles/2000GC000070/fs2000GC000070.html)

Hoernle, K. R. Werner, J. P. Morgan, D. Garbe-Schonberg, J. Bryce, and J. Mrazek, Existence of complex spatial zonation in the Galapagos plume for at least 14 m.y., *Geology*, *28*, 435–438, 2000.

Hofmann, A. W., M. D. Feigenson, and I. Raczek, Case studies on the origin of basalt, III, Petrogenesis of the Mauna Ulu eruption, Kilauea, 1969–1971, *Contrib. Mineral. Petrol.*, *88*, 24–35, 1984.

Hofmann, A. W., M. D. Feigenson, and I. Raczek, Kohala revisited, *Contrib. Mineral. Petrol.*, *95*, 114–122, 1987.

Kaneoka, I., N. Takaoka, and D. A. Clague, Noble gas systematics for coexisting glass and olivine crystals in basalts and dunite xenoliths from Loihi Seamount, *Earth Planet. Sci. Lett.*, *66*, 427–437, 1983.

Kellogg, L. H., and S. D. King, The effect of temperature dependent viscosity on the structure of new plumes in the mantle—Results of a finite element model in a spherical, axisymmetric shell, *Earth Planet. Sci. Lett.*, *148*, 13–26, 1997.

Kennedy, A. K., S.-T. Kwon, F. A. Frey, and H. B. West, The isotopic composition of postshield lavas from Mauna Kea Volcano, Hawaii, *Earth Planet. Sci. Lett.*, *103*, 339–353, 1991.

Kurz, M. D., In situ production of cosmogenic terrestrial helium and some applications to geochronology, *Geochim Cosmochim Acta*, *50*, 2855–2862, 1986.

Kurz, M. D., and D. Geist, Dynamics of the Galapagos hotspot from helium isotope geochemistry, *Geochim. Cosmochim. Acta.*, *63*, 4139–4156, 1999.

Kurz, M. D., and D. P. Kammer, Isotopic evolution of Mauna Loa Volcano, *Earth Planet. Sci. Lett.*, *103*, 257–269, 1991.

Kurz, M. D., W. J. Jenkins, and S. R. Hart, Helium isotopic systematics of oceanic islands and mantle heterogeneity, *Nature*, *297*, 43–47, 1982.

Kurz, M. D., W. J. Jenkins, S. R. Hart, and D. A. Clague, Helium isotopic variations in Loihi Seamount and the island of Hawaii, *Earth Planet. Sci. Lett.*, *66*, 388–406, 1983.

Kurz, M. D., M. O. Garcia, F. A. Frey, and P.A. O'Brien, Temporal helium isotopic variations within Hawaiian volcanoes: Basalts from Mauna Loa and Haleakala, *Geochim. Cosmochim. Acta*, *51*, 2905–2914, 1987.

Kurz, M. D., D. Colodner, T. W. Trull, R. Moore, and K. O'Brien, Cosmic ray exposure dating with in-situ produced cosmogenic ^{3}He: Results from young Hawaiian lava flows, *Earth Planet. Sci. Lett.*, *97*, 177–189, 1990.

Kurz, M. D., T. C. Kenna, D. P. Kammer, J. M. Rhodes, and M. O. Garcia, Isotopic evolution of Mauna Loa volcano: A view from the submarine southwest rift zone, in *Mauna Loa Revealed: Structure, Composition, History, and Hazards, Geophys. Monogr. Ser.*, vol. 92, edited by J.M. Rhodes and J.P. Lockwood, pp. 289–306, AGU, Washington, D. C., 1995.

Kurz, M. D., T. C. Kenna, J. C. Lassiter, and D. J. DePaolo, Helium isotopic evolution of Mauna Kea volcano: First results from the 1-km drill core, *J. Geophys. Res.*, *101*, 11,781–11,791, 1996.

Lassiter, J. C., D. J. DePaolo, and M. Tatsumoto, Isotopic evolution of Mauna Kea volcano: Results from the initial phase of the Hawaii Scientific Drilling Project, *J. Geophys. Res.*, *101*, 11,769–11,780, 1996.

Lipman, P. W., Declining growth of Mauna Loa during the last 100,000 years: Rates of lava accumulation versus gravitational subsidence, in *Mauna Loa Revealed: Structure, Composition, History, and Hazards, Geophys. Monogr. Ser.*, vol. 92, edited by J. M. Rhodes and J. P. Lockwood, pp. 45–80, AGU, Washington, D. C., 1995.

Lipman, P. W., and J. G. Moore, Mauna Loa lava-accumulation rates at the Hilo Drill Site: Formation of lava deltas during a period of declining overall volcanic growth, *J. Geophys. Res.*, *101*, 11,631–11,641, 1996.

Moore, J. G., Subsidence of the Hawaiian Ridge, *U.S. Geol. Survey Prof. Pap.*, *1350*, 85–100, 1987.

Moore, J. G., and D. A. Clague, Volcano growth and evolution of the island of Hawaii, *Geol. Soc. Am. Bull.*, *104*, 1471–1484, 1992.

Moore, J. G., B. L. Ingram, K. R. Ludwig, and D. A. Clague, Coral ages and island subsidence, Hilo drill hole, *J. Geophys. Res.*, *101*, 11,599–11,605, 1996.

Newsom, H. E., W. M. White, K. P. Jochum, and A. W. Hofmann, Siderophile and chalcophile element abundances in oceanic basalts, Pb isotope evolution and growth of the Earth's core, *Earth Planet. Sci. Lett.*, *80*, 299–313, 1986.

O'Nions, R. K., P. J. Hamilton, and N. M. Evensen, Variations in ^{143}Nd/^{144}Nd and ^{87}Sr/^{86}Sr ratios in oceanic basalts, *Earth Planet. Sci. Lett.*, *34*, 13–22, 1977.

Pietruszka, A. J., M. D. Norman, R. J. Walker, and J. W. Morgan, A rapid fluctuation in the mantle source and melting history of Kilauea Volcano inferred from the geochemistry of its historical summit lavas, *Earth Planet. Sci. Lett.*, *174*, 25–42, 1999.

Rhodes, J. M., Geochemical stratigraphy of lava flows sampled by the Hawaii Scientific Drilling Project, *J. Geophys. Res.*, *101*, 11,729–11,746, 1996.

Rhodes, J. M., and S. R. Hart, Episodic trace element and isotopic isotopic variations in historical Mauna Loa lavas: Implications for magma and plume dynamics, in *Mauna Loa Revealed: Structure, Composition, History, and Hazards, Geophys. Monogr. Ser.*, vol. 92, edited by J. M. Rhodes and J. P. Lockwood, pp. 263–288, AGU, Washington, D. C., 1995.

Ribe, N. M., and U. R. Christensen, Three-dimensional modeling of plume-lithosphere interaction, *J. Geophys. Res.*, *99*, 669–682, 1994.

Ribe, N. M., and U. R. Christensen, The dynamical origin of Hawaiian volcanism, *Earth Planet. Sci. Lett.*, *171*, 517–531, 1999.

Rison, W., and H. Craig, Helium isotopes and mantle volatiles in Loihi Seamount and Hawaiian Island basalts and xenoliths, *Earth Planet. Sci. Lett.*, *66*, 407–426, 1983.

Sharp, W. D., B. D. Turrin, P. R. Renne, and M. A. Lanphere, The ^{40}Ar/^{39}Ar and K/Ar dating of lavas from the Hilo 1-km core hole, Hawaii Scientific Drilling Project, *J. Geophys. Res.*, *101*, 11,607–11,616, 1996.

Sims, K. W. W., D. J. DePaolo, M. T. Murrell, W. S. Baldridge, S. Goldstein, D. Clague, and M. Jull, Porosity of the melting zone and variations in solid mantle upwelling rate beneath Hawaii: Inferences from ^{238}U-^{230}Th-^{226}Ra and ^{235}U-^{231}Pa, *Geochim. Cosmochim. Acta*, *63*, 4119–4138, 1999.

Spiegelman, M., and T. Elliott, Consequences of melt transport for Uranium series disequilibrium in young lavas, *Earth Planet. Sci. Lett.*, *118*, 1–20, 1993.

Staudigel, H., A. Zindler, S. R. Hart, T. Leslie, C.-Y. Chen, and D. A. Clague, The isotope systematics of a juvenile intraplate volcano: Pb, Nd, and Sr isotope ratios of basalts from Loihi Seamount, Hawaii, *Earth Planet. Sci. Lett.*, *69*, 13–29, 1984.

Steinberger, B., and R. J. O'Connell, Advection of plumes in mantle flow — Implications for hotspot motion, mantle viscosity and plume distribution, *Geophys J. Int.*, *132*, 412–434, 1998.

Stille, P., D. M. Unruh, and M. Tatsumoto, Pb, Sr, Nd, and Hf isotopic constraints on the origin of Hawaiian basalts and evidence for a unique mantle source, *Geochim. Cosmochim. Acta*, *50*, 2303–2319, 1986.

Stracke, A., Vincent J. M. Salters, Ken W. W. Sims, Assessing the presence of garnet-pyroxenite in the mantle sources of basalts through combined hafnium-neodymium-thorium isotope systematics, *Geochem. Geophys. Geosyst.*, *1*, Paper number 1999GC000013 [7832 words, 4 figures, 1 table], 1999. (Available as http://g-cubed.org/publicationsfinal/articles/1999GC000013/fs1999GC000013.html)

Todt, W., R. A. Cliff, A. Hanser, and A. W. Hofmann,

Evaluation of a ^{202}Pb-^{205}Pb double spike for high-precision lead isotope analysis in Earth processes, in *Reading the Isotopic Code, Geophys. Monogr. Ser.*, vol. 95, edited by A. Basu and S. Hart, pp. 429–437, AGU, Washington, D. C., 1996.

van Keken, P., Evolution of starting mantle plumes—A comparison between numerical and laboratory models, *Earth Planet. Sci. Lett.*, *148*, 1–11, 1997.

Walter, M., Melting of garnet peridotite and the origin of komatiite and depleted lithosphere, *J. Petrol.*, *39*, 21–60, 1998.

Watson, S., and D. P. McKenzie, Melt generation by plumes: a study of Hawaiian volcanism, *J. Petrol.*, *32*, 501–537, 1991.

Wessel, P., and L. A. Kroenke, A geometric technique for relocating hotspots and refining absolute plate motions, *Nature*, *387*, 365–369, 1997.

West, H. B., M. O. Garcia, F. A. Frey, and A. K. Kennedy, Nature and cause of compositional variation among the alkalic cap lavas of Mauna Kea Volcano, Hawaii, *Contrib. Mineral. Petrol.*, *100*, 383–397, 1988.

White, W. M., and A. W. Hofmann, Sr and Nd isotope geochemistry of oceanic basalts and mantle evolution, *Nature*, *296*, 821–825, 1982.